HIGH VELOCITY IMPACT STUDIES ON S-2 GLASS LAMINATED COMPOSITES

Thesis

Submitted to

The Mechanical Engineering Department of the

UNIVERSITY OF DAYTON

In Partial Fulfillment of the Requirements for

The Degree

Master of Science in Mechanical Engineering

by

Kandasamy Rathnam

UNIVERSITY OF DAYTON

Dayton, Ohio

August, 1994

HIGH VELOCITY IMPACT STUDIES ON S-2 GLASS LAMINATED COMPOSITES

APPROVED BY:

James M. Whitney, Ph.D.
Graduate Material Engineering

N. S. Brar, Ph.D.
Physicist Impact Physics Group
Experimental Mechanics
Research Institute

James A. Snide, Ph.D.
Material Engineering Department

Donald L. Moon, Ph.D.
Associate Dean/Director
Graduate Engineering & Research
School of Engineering

Joseph Lestingi, D.Eng., P.E.
Dean
School of Engineering

ABSTRACT

HIGH VELOCITY IMPACT STUDIES ON S-2 GLASS LAMINATED COMPOSITES

Kandasamy Rathnam
University of Dayton, August, 1994

Advisor: Dr. N.S. Brar

Post failure analysis of the impacted 12.7 mm thick S-2 glass composite panels (150x150 mm) was performed to study the failure modes during penetration. The panels were impacted projectiles (4.5 g) with three different nose shapes (blunt, conical and hemispherical) at velocities 250-600 m/s and impact data was reported in an earlier study. The back-face deflection of the laminates was also recorded in that study with the Imacon high speed camera at 10^5 f/s. Post failure analysis revealed that the laminates failed during penetration by cratering due to punching of fibers, laminate crushing, delamination and fiber stretching and breaking. The extent of failure modes varied with strike velocity of the projectile. Stress based failure criteria were proposed for these failure modes. Impact of the blunt nose projectiles on to S-2 glass laminate was simulated by incorporating the failure criteria in DYNA3D code. Simulated ballistic limit of the laminate and residual velocities of the blunt nose projectiles agreed within 10% of the experimental results. However, the same failure criteria failed to predict the ballistic limit of 6.4 mm thick S-2 glass laminates impacted by 5.8, 17, and 44 grain projectiles.

DEDICATION

To my family and friends

ACKNOWLEDGMENTS

I express my sincere gratitude to my thesis advisor, Dr. N. S. Brar, for his guidance and continuous support throughout this research. I also acknowledge Dr. James Whitney and Dr. James Snide for serving on my thesis committee. Dr. A. M. Rajendran of Army Research Laboratory, and Dr. Gallagher are thanked for financial support during initial part of this program, and also I thank Dr. Robert Brockman for helpful technical discussions. Special thanks are also due to Mr. Dave Grove for assisting me in the use of DYNA3D, and Mr. Dick Tocci for helping me with photographs, and Dr. Reji John for friendly help.

Above all, I extend my deepest appreciation to my wife, Lakshmi, my son, Roopak, and my daughter, Deepika, for their understanding, and love and my parents and my in-laws, without whose love and prayer this would never have come true.

TABLE OF CONTENTS

LIST OF FIGURES

LIST OF TABLES

CHAPTER I

INTRODUCTION

1.1 IMPORTANCE OF CURRENT RESEARCH

A composite material consists of two or more materials, which are physically distinct and mechanically separable substances. The desired properties can be achieved by mixing the substances in a controlled way. Fiber composites exhibit high strength, high stiffness, better life and light weight, are obtained by bonding the laminates of one or two materials together. These properties combined with flexibility in design and ease of manufacturing have established composites as one of the advanced engineering materials. They have been developed as protective shield for the space vehicles, personnel carriers, helicopter or human body armor to protect against the penetration of projectiles and fragments. Also, composite materials are used as containment rings in aircraft engines to contain turbine blade fragments. Composite materials absorb more kinetic energy compared to conventional armor materials for the same areal density.

The failure and damage encountered in components on impact are more complicated than for isotropic materials. The common failure modes in metallic plates subjected to impact of projectile includes, spalling, cratering, piercing, bulging, dishing, and petalling [1]. For composite laminates pierced by a projectile involves additional failure process such as delamination, debonding of fiber and matrix and fiber pullout, stretching and failure. Due to these complex failure modes in laminates during penetration together with anisotropic nature of composites, make analytical modeling of composites

penetration very difficult. Hence, accurate modeling of impact phenomena on composite laminates through finite element simulations is a important tool to predict the ballistic limit, that is, the velocity at which the projectiles have a 50% probability of perforating targets and residual velocity of the projectile.

1.2 RESEARCH OBJECTIVES

The objectives of the current research are to observe the failure modes in 12.7 mm thick woven S-2 glass laminates below and above the ballistic limits of the laminate, impacted by projectiles with three different nose (blunt, conical and hemispherical) shapes in the velocity range 300 to 650 m/s, to propose failure criteria for the observed failure modes, and to predict the ballistic limit of the target and residual velocities of blunt nose projectile from numerical simulations using Chang-Chang failure criteria existing in DYNA3D and proposed failure criteria based on the observed failure modes.

1.3 RESEARCH APPROACH

S-2 glass laminates of 12.7 mm thick laminates impacted by projectiles with three different nose shapes (blunt nose, conical nose and hemispherical nose) are examined to identify the failure modes for velocities below and above the ballistic limit of the targets. A stress based failure criteria are proposed based on observed failure modes. The proposed failure criteria are incorporated in DYNA3D code. The impact event is numerically modeled using DYNA3D. Ballistic limit of the laminates and residual velocities of the projectile are simulated using the proposed failure criteria and Chang-Chang failure criteria. The results from these failure criteria are compared with the experimental results. In addition simulations are performed on 6.4 mm laminates impacted by 5.8, 17, and 44 grain FSPs to check the validity of the proposed failure criteria.

1.4 THESIS ORGANIZATION

The remainder of the thesis is organized as follows. In Chapter II, previously published research on penetration studies is reviewed. The review include penetration model and ballistic limit, penetration studies on isotropic materials, penetration studies on composite materials, factors and affect energy absorption of composite materials. Chapter III present the experimental investigations, which include experimental description, observed failure modes and back face deflection of the laminates. Failure criteria for composite laminates have been reviewed and proposed failure criteria are given in Chapter IV. Numerical simulations, include description of code, modeling of steel plate impact and modeling on composite laminates are given in Chapter V. Chapter VI presents the results and discussion. The thesis conclusions and recommendations for the future research are given in Chapter VII.

CHAPTER II
PENETRATION STUDIES

2.1. PENETRATION MODEL AND BALLISTIC LIMIT

A number of models have been proposed to predict the behavior of the materials under impact penetration. Zukas et al. reviewed and discussed the proposed impact penetration models [2, 3]. The most commonly used form of the impact penetration model is actually based on a semi-empirical model and is derived from energy balance and certain empirically determined parameters. Once the residual velocity of the projectile after complete penetration through the target is predicted by the model, the total energy absorbed by the target can be obtained. Most of the models comply to a general form:

$$V_r = \alpha(V_s^p - V_s^p)^{\frac{1}{p}}, V_s > V_l \quad (1)$$

where V_r = penetrator residual velocity
V_s = penetrator striking velocity
V_l = limit velocity, a material parameter
α, p = empirical constants

The general form listed above is actually a modification of the energy balance equation. The total energy loss U for the projectile is

$$U = \frac{1}{2} m(V_s^2 - V_r^2) \quad (2)$$

The maximum energy that the material dissipates, W can be written as:

$$W = 1/2\, m\, V_l^2 \quad (3)$$

Equating the two energy expressions, for U and W, we get,:

$$V_r = (V_s^2 - V_l^2)^{\frac{1}{2}} \quad (4)$$

The major deficiency of the this model is that the mechanisms of energy dissipation process can not be evaluated. The model treats the target (composite or metallic) material as a whole, and the parameters to predict the final velocity of the projectile after impact are experimentally determined. The contributions from the constituents of the composite laminates such as fiber, matrix, and their interface towards the total absorbed energy cannot be separated.

2.2. PENETRATION STUDIES ON ISOTROPIC MATERIALS

A complete survey of ballistic penetration and perforation of conventional materials can be obtained from the paper of Backman and Goldsmith [1] and Zukas et al. [2, 3]. The common damage and failure modes encountered during penetration processes in thin targets include spalling, cratering, piercing, dishing, and petalling. These are shown in Figure 1 [3]. The damage mechanisms depend on the property of the target material, structure and the incident angle of the projectile. As the strike velocity increases the response of the structure become secondary to behavior of the material within the small zone of the impact area. The material constitution, strain rate, localized plastic flow and failure are manifested at different stages of the impact process. A number of models have been developed to account for these different processes during penetration. But, no unique theory is developed to account for the variety of target responses encountered under the different impact conditions.

The computational approach using finite element and finite difference method is reviewed by Zukas et al. [2,3] and Anderson and Bonder [4]. The survey of computer codes available for impact simulation is reviewed by Zukas [3] and Anderson has reviewed the theory of hydrocodes [5].

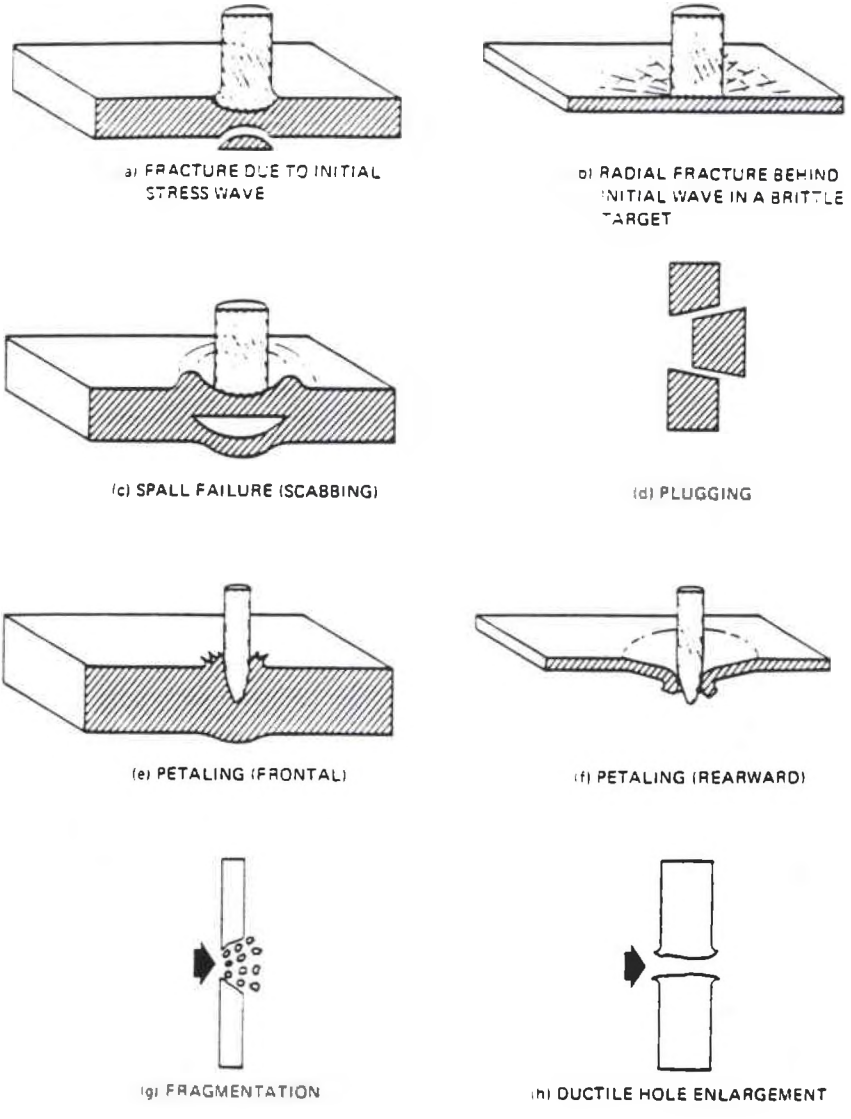

Figure 1. Perforation Mechanisms [1].

2.3 PENETRATION STUDIES ON COMPOSITE MATERIALS

2.3.1. Experimental Investigations

For the last two decades, penetration of composite laminates have been studied using fragment simulating projectiles [6-15], blunt nose cylindrical projectiles [11, 16] and conical nose projectiles [17, 18]. Most of these studies are experiments [6-15] and in some cases the ballistic performance is compared with that of isotropic materials [12]. The composite laminates degraded during the penetration of the projectile. The degradation of laminates leads to a number of failure and damage mechanisms. The primary failure mechanisms encountered by the fibers of the composites are: 1. lateral displacement of fibers, 2. breaking of fibers in shear and 3. strain and break the fiber in tension as shown in Figure 2 [6].

Other failure modes, such as delamination, interlaminar failure, matrix cracking and debonding of fiber and matrix are also participate during penetration. These failure modes and the damage mechanisms vary depending on the fiber/matrix combination, type of projectile and its striking velocity. For example, when a blunt nosed projectile penetrated into a carbon/epoxy composite, the damage and failure mechanisms were matrix cracking, delamination and fiber failure [16]. On the other hand, spectra, kevlar and glass fiber composites, which are not as brittle as carbon fiber composite, have different failure and damage mechanisms such as fiber stretching and breakage and debonding of laminates dominate the penetration process [6].

Cartwell studied the influence of the geometrical parameters on unidirectional GFRP composites with different lay-up sequence impacted by sphere projectiles for strike velocities ranging from 10 m/s to 500 m/s using a high pressure nitrogen gas gun [7]. He studied the change of failure modes with geometrical parameters (length, width and thickness of the laminates). In the low velocity range the geometry of the laminates had influence on the projectile kinetic energy absorption, but at higher velocities the laminate's geometry did not have any influence on energy absorption.

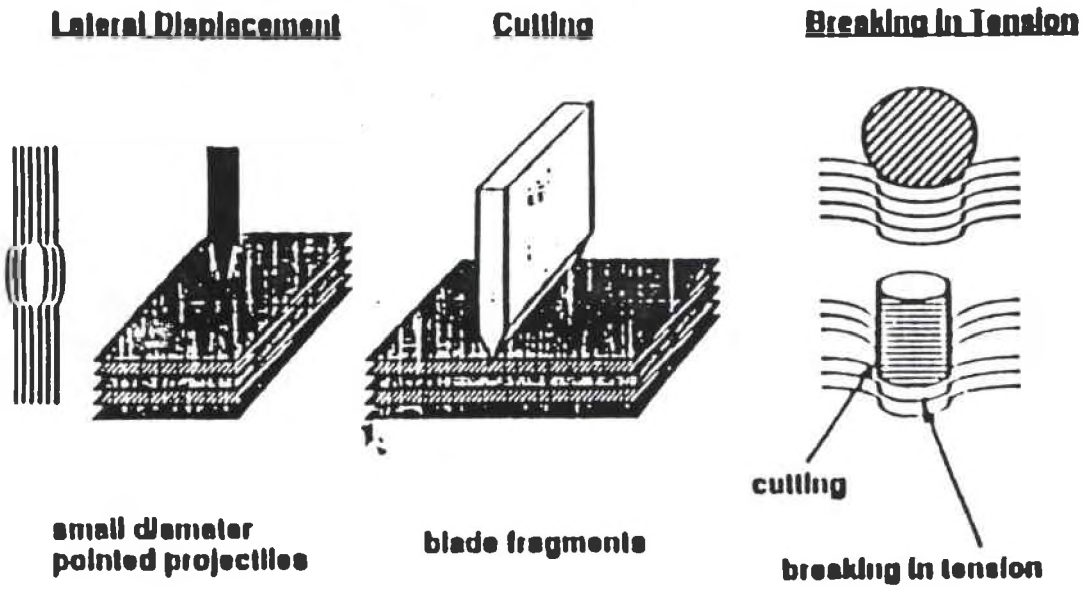

Figure 2. Principal failure mechanisms in penetration of composite laminates [6].

Cristescu et al. [18] discussed failure mechanisms in composite laminates struck by blunt nosed projectiles. The failure mechanisms included shear cut-out of plug, fiber debonding, fiber stretching, fiber breaking, matrix deformation and matrix cracking. They studied delamination processes in the laminates during penetration of a flat nose projectile and concluded that delamination was an important failure mechanism. Later studies indicated that delamination is an important failure mechanism in brittle composites such as carbon/epoxy laminates and not in polyethylene, kevlar and glass fiber composites [6].

2.3.2 Analytical Modeling of Composites in Penetration

Analytical modeling of penetration process in composite laminates is extremely difficult due to a number of failure modes participating during penetration, together with anisotropic nature of composite laminates. Zhu [9] developed a three stage (indentation, penetration, and exit) phenomenological model for a cylindero-conical projectile penetrating into woven kevlar/polyester laminates based on existing theories from isotropic materials. The force from the quasi-static punch test and maximum strain to failure of the fiber was used as failure criteria. The predictions from the model agreed with measurements for strike velocities near the ballistic limit of the laminates. Predicted residual velocities of the projectile above the ballistic limit of the laminates agreed only within 30% of the measurements. This is likely due to the fact the same models were used for below and above the ballistic limit the laminates. The limitation of the model is that it can not be used for any other type of projectiles.

Lin and Bhatnagar [20] developed a empirical model to predict the critical energy of the FSP penetrating into spectra fiber using the experimental results. Cantwell and Morton developed a simple model to predict the perforation threshold of carbon/epoxy composites beam, and the predictions from the model agreed well with measured values for target thickness up to 4 mm [19].

2.3.3 Numerical Simulations of Penetration in Composites

Lee and Sun identified the failure modes in 2 mm graphite/epoxy laminates from static punch tests using rigid blunt nose cylindrical rod and the dynamic penetration of a blunt nosed projectile in the velocity range 25 to 80 m/s, to be matrix cracking, delamination and plugging, [16]. In the simulation they assumed that initiation of matrix cracking occurred when the stress perpendicular to fiber direction reached its tensile strength value and as a consequence delamination took place. This model is valid only for one thickness of laminates, since failure modes change with thickness of carbon composite laminates and strike velocity of the projectile [7]. Prevorsek et al. [6] studied the deformation behavior of unidirectional Spectra fiber impacted by a projectile and observed that the fiber breakage in shear (transverse) absorbed 10% of total kinetic energy of the projectile. This shows the need for describing a failure criteria due to transverse shear during penetration of laminates.

Blanas [21] modeled and simulated the ballistic limits of the woven composite targets (E-glass/epoxy resin, S-2 glass/typical resin type and kevlar-29/polyester resin) impacted by fragment simulated projectiles (FSP) velocities in the range 300 to 700 m/s using DYNA3D. Chang-Chang failure criteria for fiber failure, matrix failure and matrix crushing available in DYNA3D [22] were used. The predicted ballistic limit of the FSP with 44 grains (1 g = 15.4 grains) on S-2 glass was 15 to 50% lower than the experimental values. The agreement between the simulated and measured ballistic limit improved in thicker laminates. The simulated ballistic limit of 5.85 grain FSP on S-2 glass laminate was 7% to 37% higher than the experimental results. The likely reasons for this disagreement are : the inplane stresses σ_{xx}, σ_{yy} and σ_{xy} are used in predicting the failure, which are not the case in impact penetration studies, since the loading is normal to the fiber. The transverse shear stresses σ_{zx}, and the normal stress σ_{zz} play dominant role compared to the normal stresses σ_{xx} and σ_{yy} in penetration process. The failure mode changes with target thickness and size of the projectile. We observed two different sets of

failure modes for strike velocities below and above the ballistic limit and are discussed in Chapter III.

2.4. IMPACT ENERGY ABSORPTION IN COMPOSITE LAMINATES

The energy absorbed by the composite laminate depends on the projectile nose shape and its strike velocity; type of composite material, and thickness of the laminates. Hsieh et al. [17] studied the energy loss profile of three types woven composites, spectra, kevlar-49 and graphite fibers with epoxy resin impacted by a cylindero-conical projectile. Microvelocity sensor was used to measure the deceleration of the projectile during dynamic penetration at a strike velocity of about 250 m/s. Figure 3 shows the energy loss profile for three composites and three different thicknesses made up of 10, 20 and 30 plies of laminates subjected to low and high velocity impact. From their study they did not conclude the effect of laminate thickness on energy absorption, since the study was limited to only three laminate thickness. However, increase in thickness showed increase in projectile kinetic energy absorption of the composite laminate (Figure 3).

Zhu [18] studied the effect of thickness with different lay-up of woven kevlar laminates and conical nose penetrator from static punch tests. The energy absorbed by the laminates increased and also the maximum force during static penetration tests increased non-linearly with increase in thickness of the laminates. On the other hand the stacking sequence of woven kevlar laminates did not exhibit any effect on terminal velocity of the projectile. The energy absorbed by the laminates during dynamic penetration is shown in Figure 4.

Delamination is one of the important failure mechanisms in the laminates during projectile penetration and the role of delamination in energy absorption of the laminates is still not well understood. However, the induced delamination in woven kevlar laminates did not show any effect on terminal velocities of the projectile for impact velocity in the range as shown in Figure 5. On the contrary, the artificially delaminated woven kevlar

laminates absorbed 10% less energy compared to that absorbed in intact laminates under static penetration [18]. The other failure mechanisms for example matrix cracking, and interlaminar shear did not absorb significant energy. This may be due to the fact that temperature of the laminates being penetrated rises thus lowering the tensile and compressive stress of the matrix. However, these failure mechanisms may be important at low velocity impact.

During penetration, the laminates are subjected to a high strain rate loading and that is likely to change laminates properties such as Young's modulus, tensile strength and failure strain. These properties have effect on the terminal velocities of the projectile of woven kevlar laminates as shown in Figures 6 (a) and (b) [18].

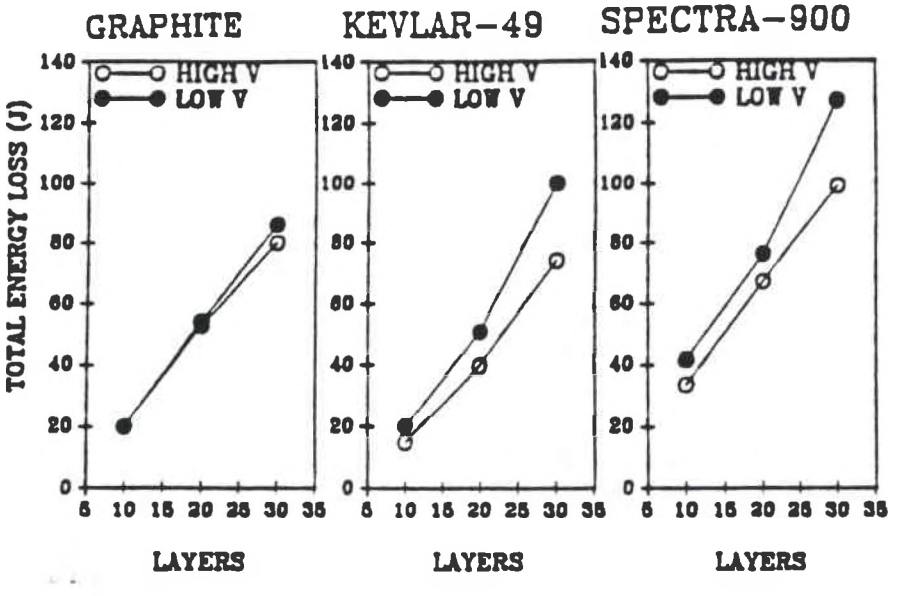

Figure 3. Total energy loss for 10, 20, and 30 plies of Polyethylene, Kevlar, and Graphite composites at different velocities [17].

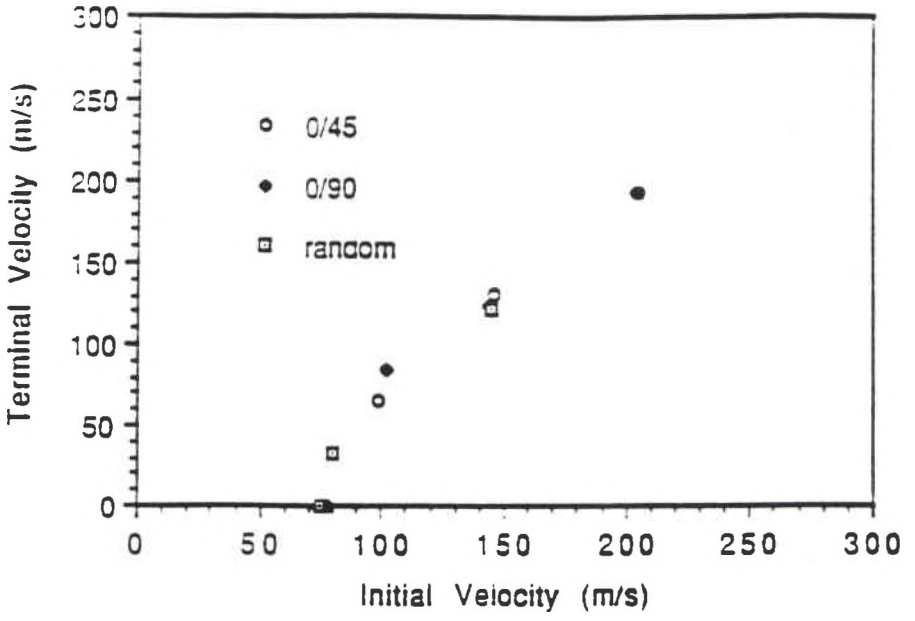

Figure 4. Perforation of 5 ply laminates with different lay-up by a 12.7 mm diameter conical nose projectile [18]

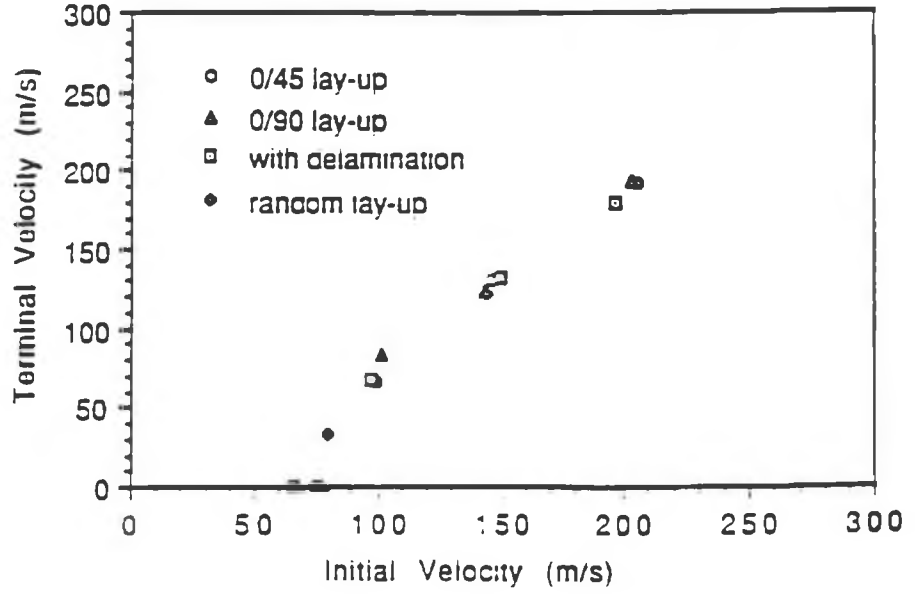

Figure 5. Comparison of terminal velocities of 5 ply laminates with and without artificial delamination [18].

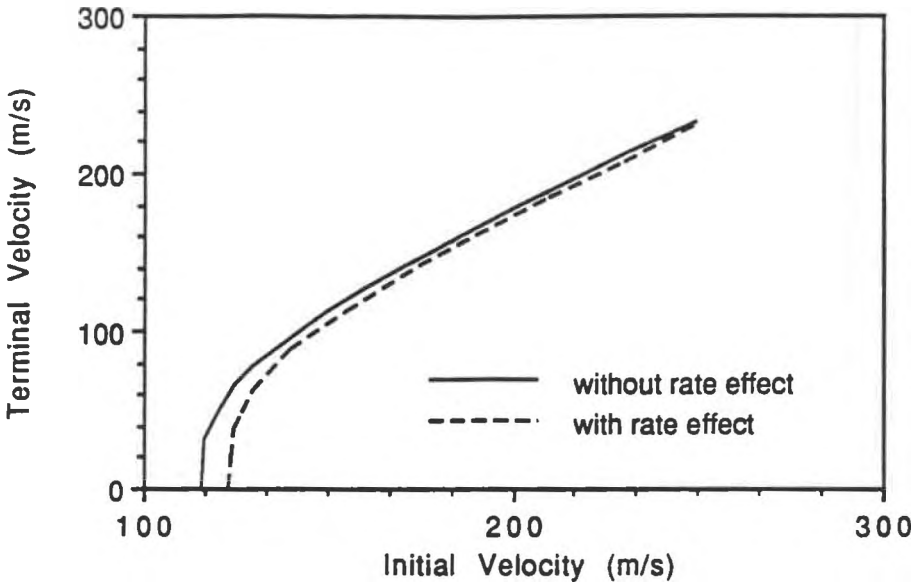

Figure 6 (a). Comparison of terminal velocities as a function of strain rate of woven kevlar laminates [18].

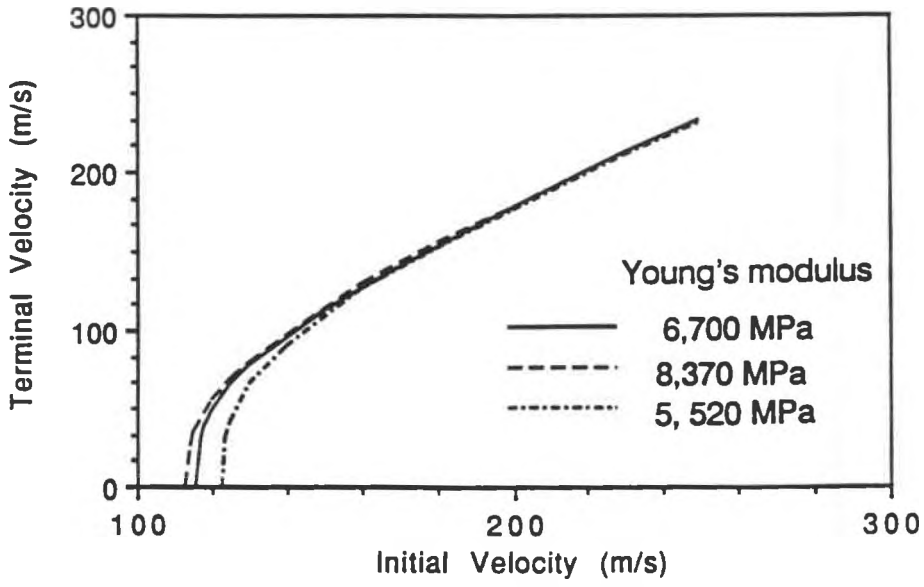

Figure 6 (b). Comparison of terminal velocities for different Young's modulii laminates [18].

CHAPTER III

EXPERIMENTAL TECHIQUES AND RESULTS

3.1 EXPERIMENTAL DESCRIPTION

In the present study the shot woven 12.7 mm thick S-2 glass fiber and phenolic resin laminates in an earlier study [10] are examined to identify the failure modes in the laminates below and above the ballistic limit and to measure the back-face deflection of the laminate during penetration. The laminates used in the experiment measured 150x150x12.7 mm and all edges were clamped in the target fixture.

Modified 7.9 mm caliber fragment simulating projectiles (FSPs) as per MIL-P-46593 were used Three types of nose shapes, a cone with apex ratio 3, a hemispherical and a flat right circular cylinder as shown in Figure 7, were employed in this study. A tail was added to the projectile in order to measure the declaration of the projectile. All projectiles were made from SAE 4340 steel as per MIL-S-5000E, and the hardness was 30 ± 1 HRC.

A total number of 28 experiments were performed on S-2 glass laminates employing all three types of projectile and the shot data are summarized in Table 1. The residual velocities of the projectile were measured from 18 experiments and back-face deflection was measured in all the experiments using the Imacon high speed camera at a framing rate 10^5f/s. The laminates were sliced into two pieces by sawing the cavity/crater left by the penetrator. The cross section of the sawed surfaces were photographed to study the failure modes at striking velocities below and above the ballistic limit.

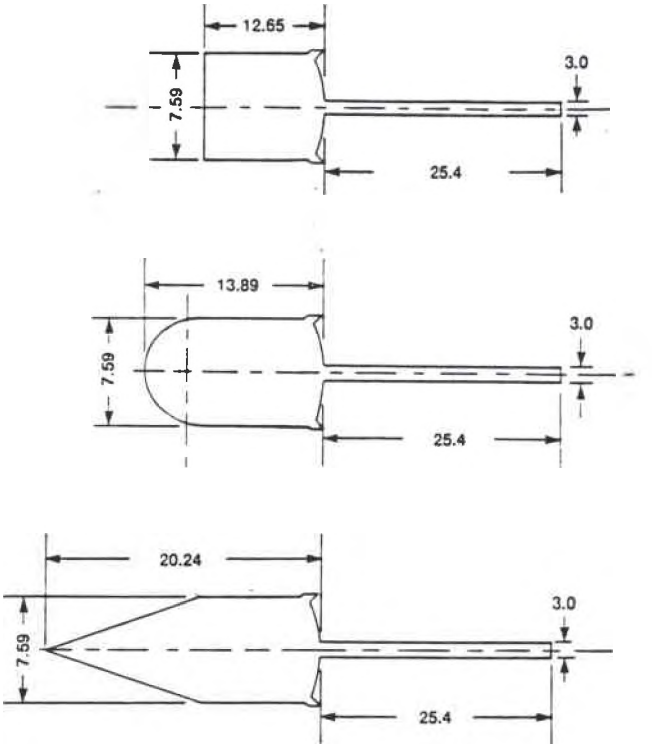

Figure 7. Projectile geometry (dimensions in mm)

Table 1

Summary of Shot Data [11]

Shot No.	Projectile Type	Strike Velocity (m/s)	Residual Velocity (m/s)
6-2202	conical	243	0
6-2204	conical	283	0
6-2216	conical	314	0
6-2217	conical	326	0
6-2203	conical	327	120
6-2218	conical	351	89
6-2220	conical	357	0
6-2219	conical	361	79
6-2221	conical	373	-
6-2201	conical	380	110
6-2200	conical	451	283
6-2197	conical	484	-
6-2199	conical	545	-
6-2207	Hemispherical	349	0
6-2223	Hemispherical	400	91
6-2208	Hemispherical	411	88
6-2206	Hemispherical	424	138
6-2222	Hemispherical	444	-
6-2189	Hemispherical	473	-
6-2190	Hemispherical	478	-
6-2209	Blunt	466	0
6-2210	Blunt	520	0
6-2211	Blunt	547	86
6-2213	Blunt	571	310
6-2196	Blunt	602	-
6-2195	Blunt	612	-

3.2 OBSERVED FAILURE MODES

The general, for all three nose shape projectile penetrated into composite laminates by shearing the laminates and as a result forming a crater in the laminates immediately after the impact shown in Figure 8 (a), 8 (b) and 8 (c) for the blunt, hemispherical and conical nose projectiles respectively. This is accompanied by delamination through the thickness and bulging towards the back side of the laminates. The particular failure modes for each nose shape of the projectiles are different. The blunt nose projectile shears the fibers around the edge and creates a large crater. As a result the laminates absorb more energy and the ballistic limit for this projectile is high (533 ± 13 m/s). In contrast, conical and hemispherical nose projectiles shear the fibers only at the tip of the nose and the sheared fibers are pushed radially around the projectile, and fibers kink and buckle laterally. The broken fibers are displaced above the target surface (Figure 8 (b) and Figure 8(c)). The ballistic limits of conical nose (342 ± 15 m/s) and hemispherical nose (374 ± 26 m/s) are lower than that for the blunt nose projectile. The common failure modes observed in the laminates below the ballistic limit are cratering, laminate crushing and delamination of laminates.

Increase in strike velocity changes the nature of failure mode in the laminates. The photographs of the laminates penetrated at strike velocity above the ballistic limit are shown in Figure 9 (a), 9 (b) and 9 (c) for flat, hemisphere, and cone nose projectiles respectively. The projectile stretches, shears and pushes the fibers through the back side of the laminates for velocities above complete penetration. A crater forms on the strike face of the target and the cratering is predominant in the case of blunt nose projectiles. Also, the flat nosed projectile stretches, breaks, and shears the fibers in larger area ahead of the projectile compare to the other nose shapes.

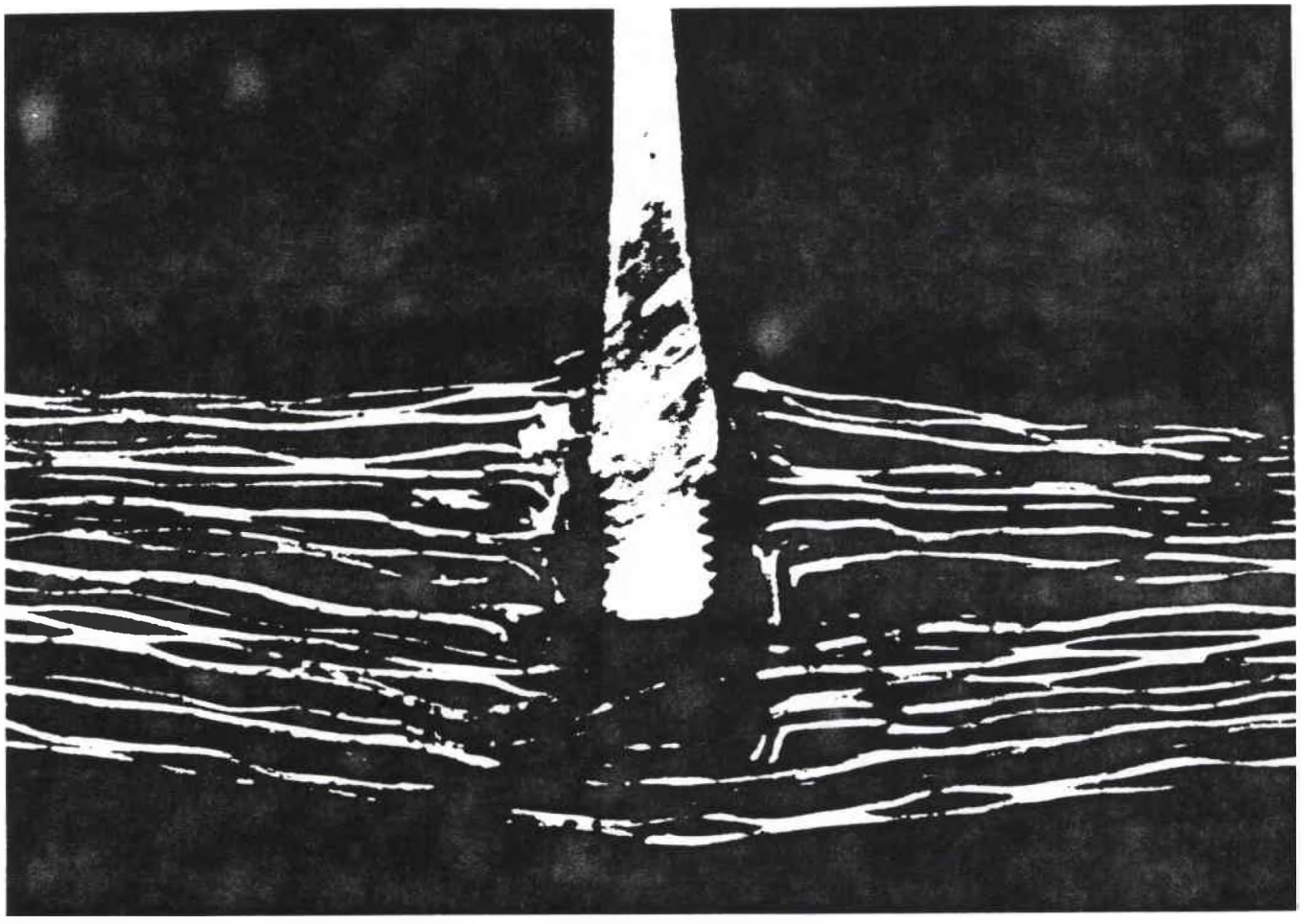

Figure 8 (a). Partial penetration of S-2 glass composite panel by a blunt nose projectile at 466 m/s.

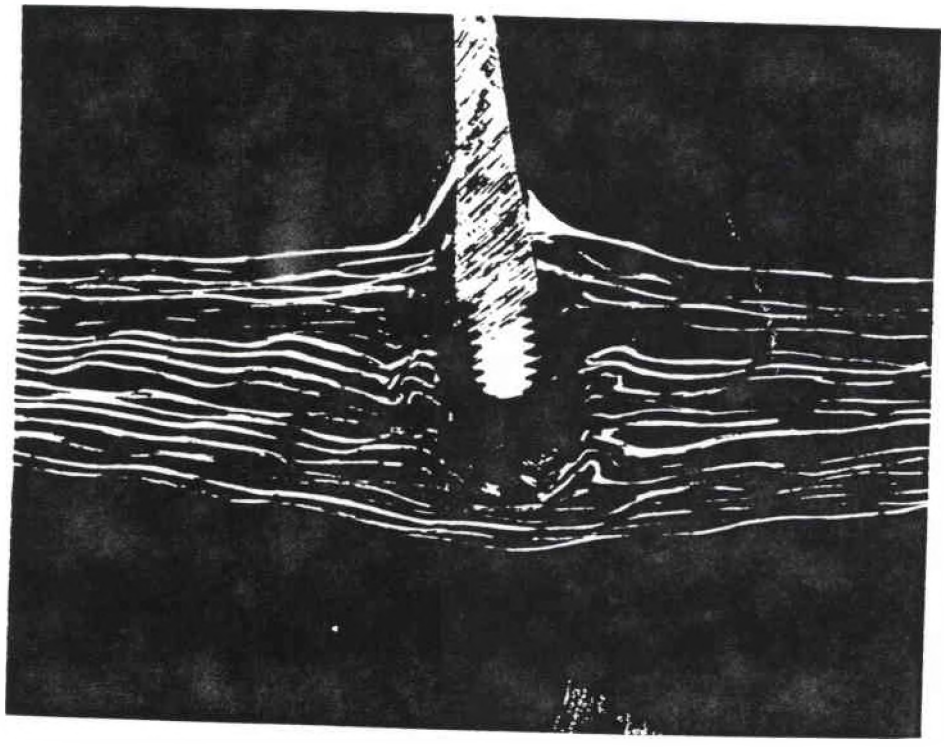

Figure 8 (b). Partial penetration of S-2 glass composite panel by a hemispherical nose projectile at 349 m/s.

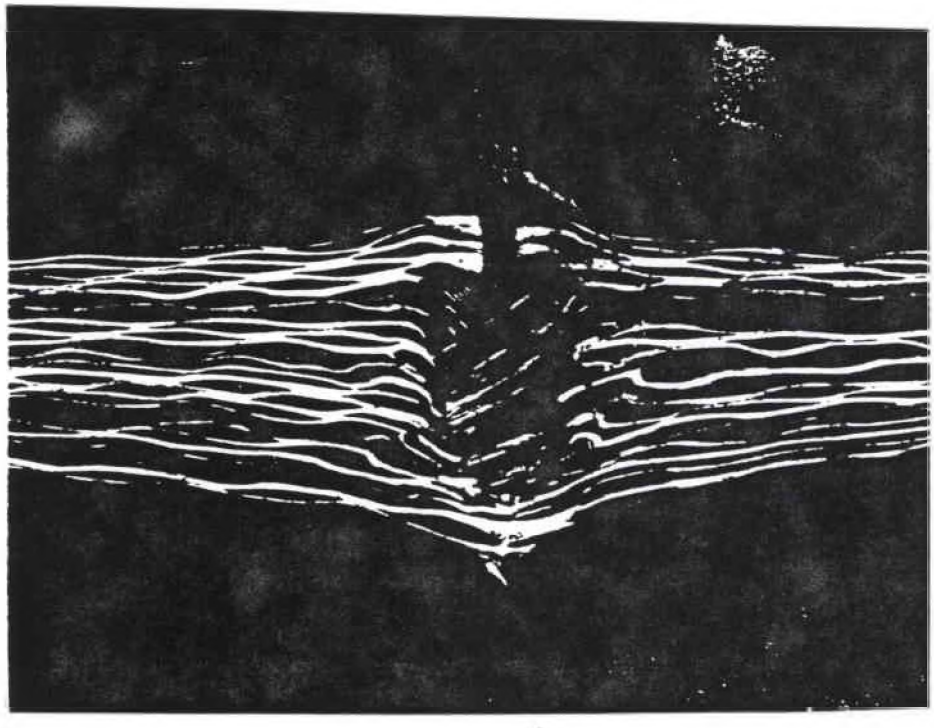

Figure 8 (c). Partial penetration of S-2 glass composite panel by a conical nose projectile at 327 m/s.

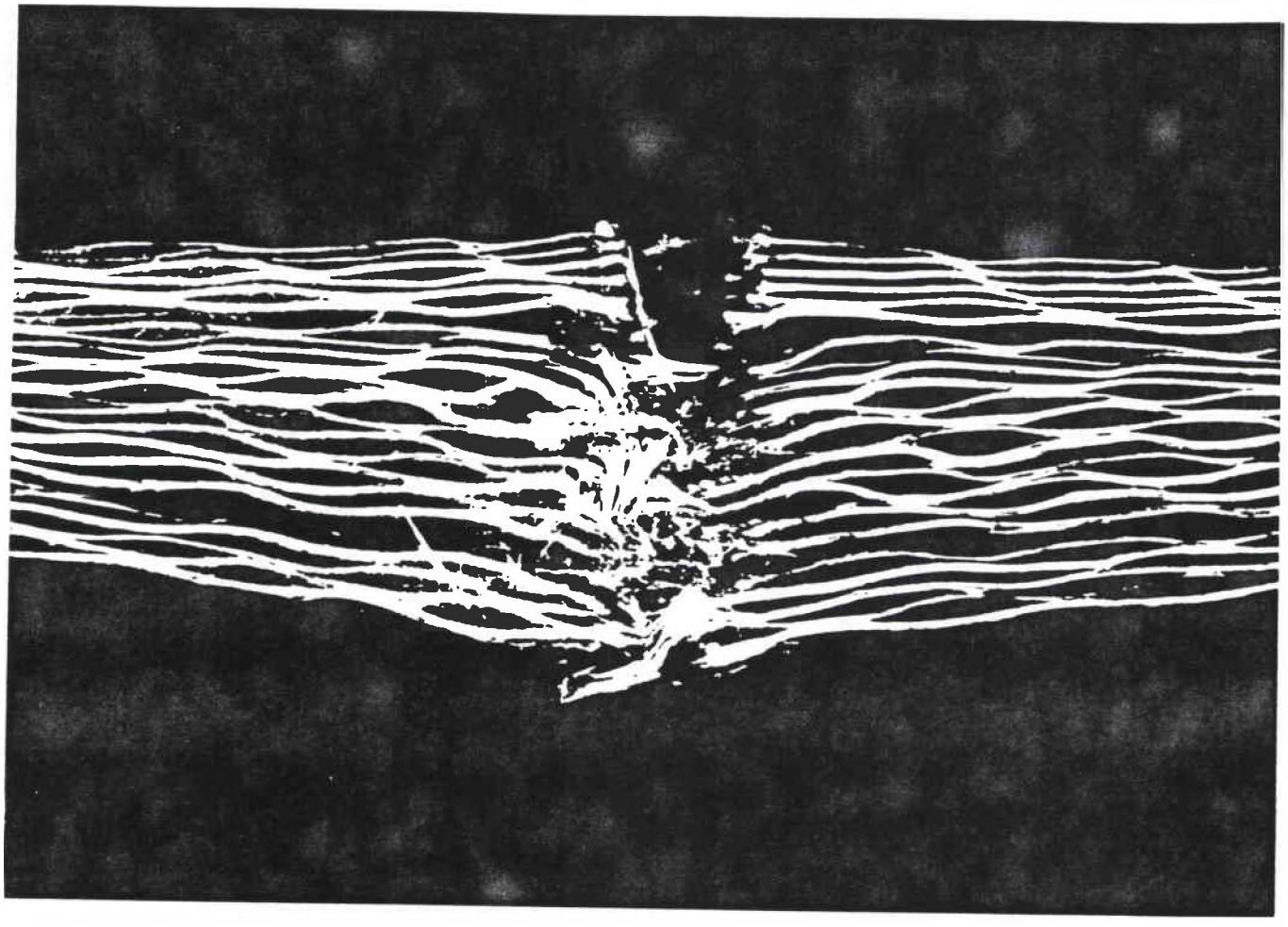

Figure 9 (a). Complete penetration of S-2 glass composite panel by a blunt nose projectile at 520 m/s.

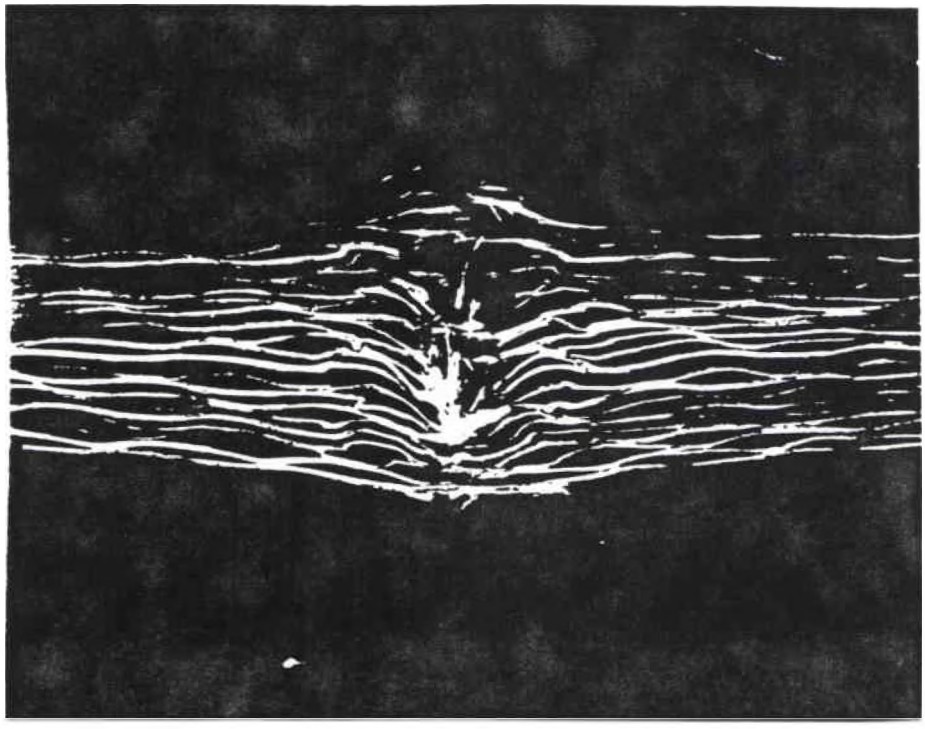

Figure 9 (b). Complete penetration of S-2 glass composite panel by a hemispherical nose projectile at 349 m/s.

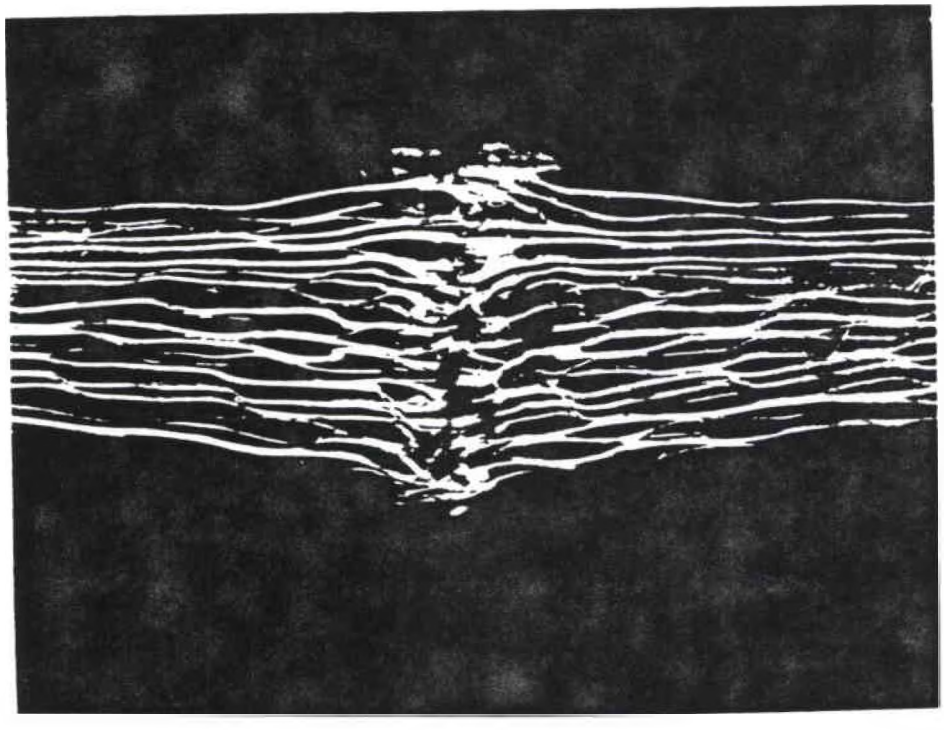

Figure 9 (c). Complete penetration of S-2 glass composite panel by a conical nose projectile at 361 m/s.

The depth of the crater decreases with increase in strike velocity and delamination in the laminates moves toward the rear side of the target with increase in strike velocity. Prifti et al. [15] observed a similar effect in their study on the delamination area and volume through the thickness of 44 mm thick S-2 glass laminates impacted by two type (12.7 mm and 20 mm caliber) FSPs using computed tomography. The fiber stretching and breaking are the important failure modes for the velocities above the ballistic limit of the laminates.

In summary, two different sets of failure modes are observed in the target with partial and complete penetration of the projectile. Cratering, delamination and laminate crushing are major failure modes in the laminate for velocities below the ballistic limit of the target. On the contrary, fiber stretching and breakage, delamination and cratering are the important failure modes for projectile velocities above the ballistic limit of the target. The extent of cratering decreases with increase in strike velocity.

3.3 BACK-FACE DEFLECTION OF LAMINATES

Back-face deflection of the laminates was measured for all three types, conical, hemispherical and blunt nose projectiles at different velocities, using IMACON camera. A sequence of photographs taken every 10 μs is shown in Figure 10. The back-face deflections of the laminates for blunt, hemispherical and conical nose projectiles were measured and are shown in Figures. 11 , 12 and 13 respectively.

The data on back-face deflection shown in Figures 11-12 suggests that there is no back-face deflection of the panels for the first 20 μs after impact. Furthermore, the bulging is very local around the penetrator cavity. The deflection of the laminates increases with increase in projectile strike velocity up to the ballistic limit of the target and remains almost constant above complete penetration of the target. Below the ballistic limit the bulging of the laminates around the penetrator cavity is also a function of projectile shape. The conical nose projectile pierced the laminates at the nose tip and

paves way for the projectile to move fast therefore results in less bulging. Blunt and hemispherical projectiles produce larger bulging in the laminates compared to conical nose projectile.

The back-face deflection or bulging of the laminates impacted by projectile of all three nose shapes above the ballistic limit are shown in Figure 14. The deflection from the conical nose projectile is 40% lower those for blunt and hemispherical nose projectiles. The extent of the absorption of the kinetic energy of the projectile due to bulging of the composite panels during penetration is not known and needs to be investigated.

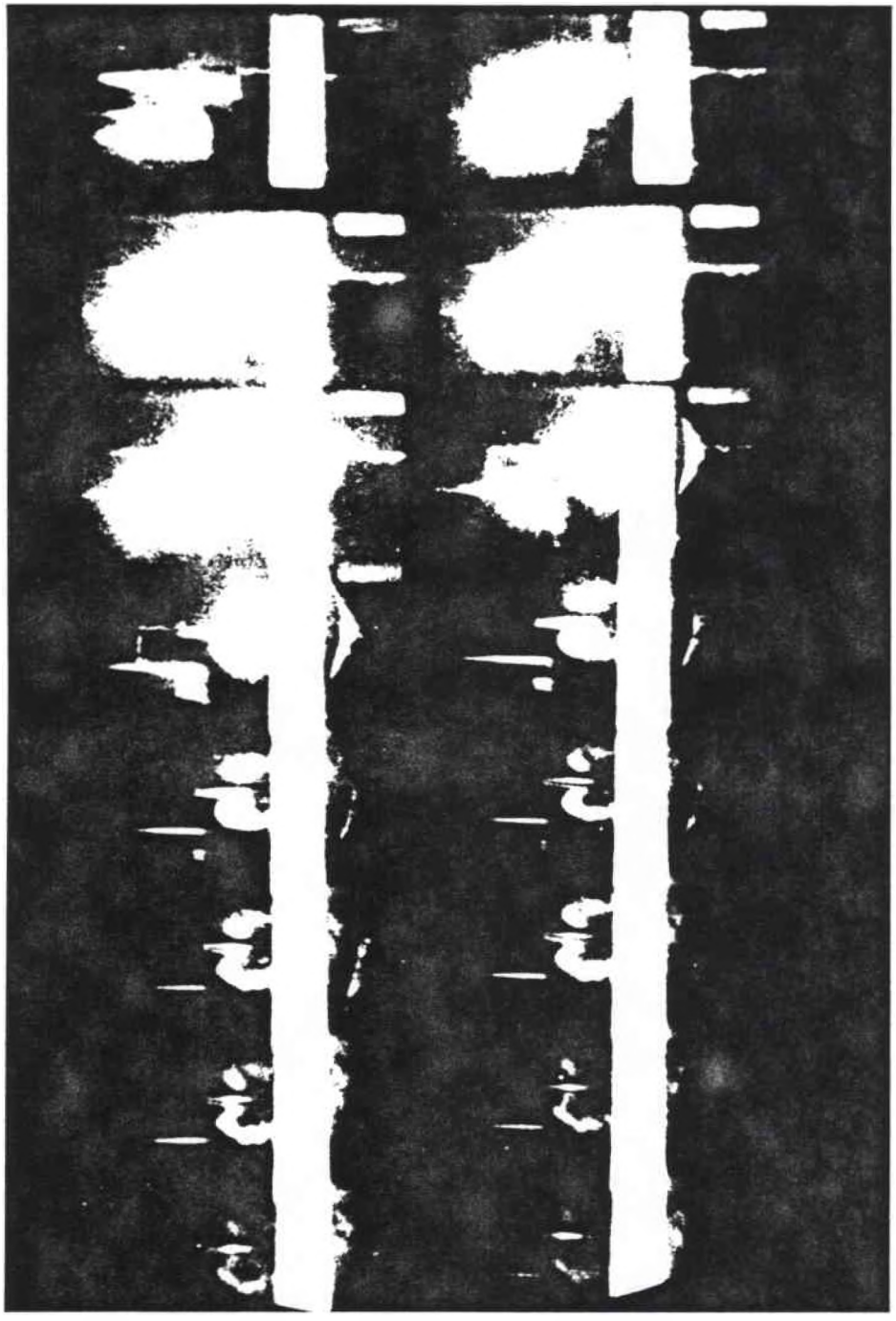

Figure 10. A sequence of photographs of a blunt nose projectile penetrating into S-2 glass laminates taken at every 10 μs.

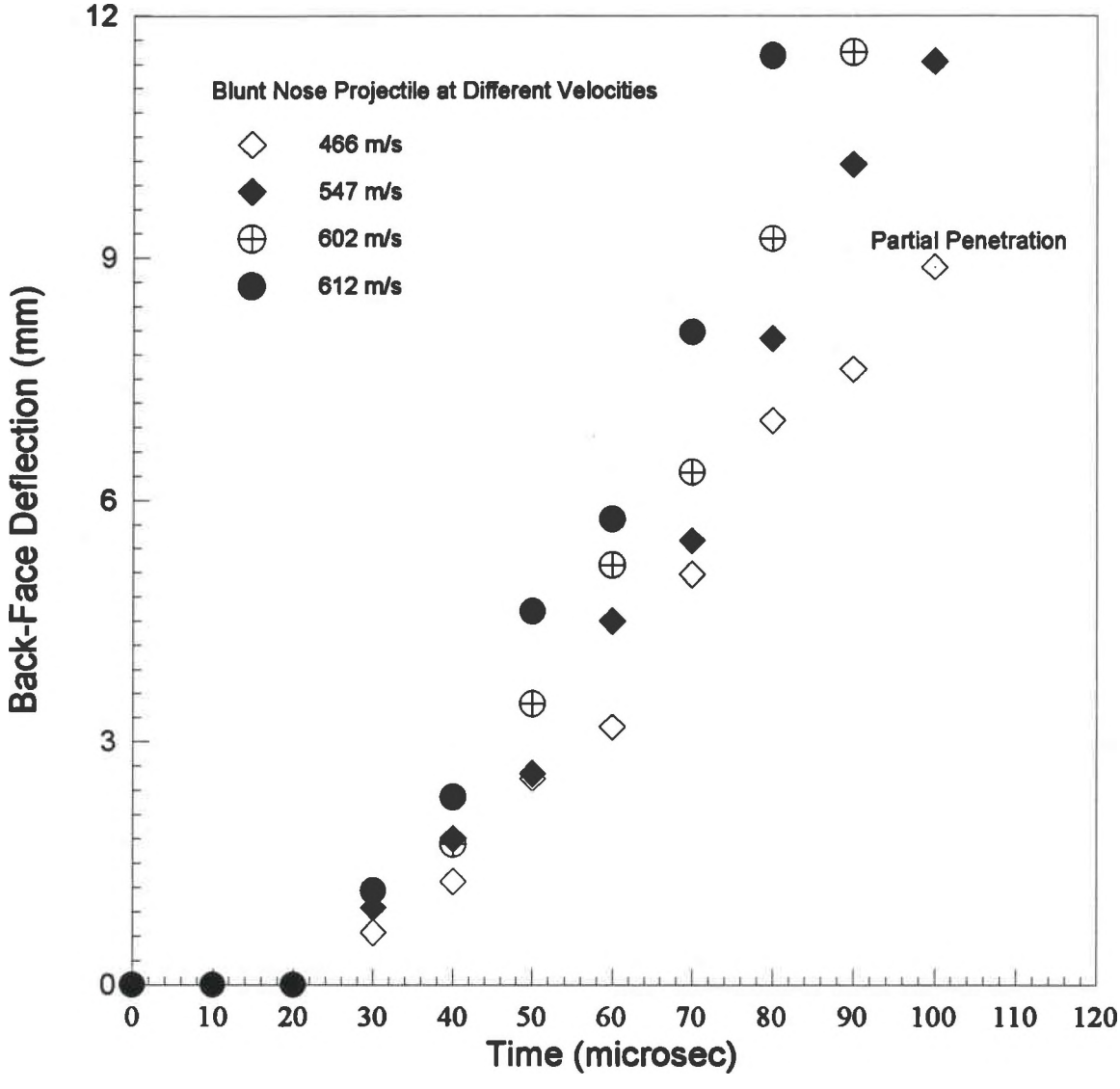

Figure 11. Back-face deflection of S-2 glass laminates impacted by a blunt nose projectile.

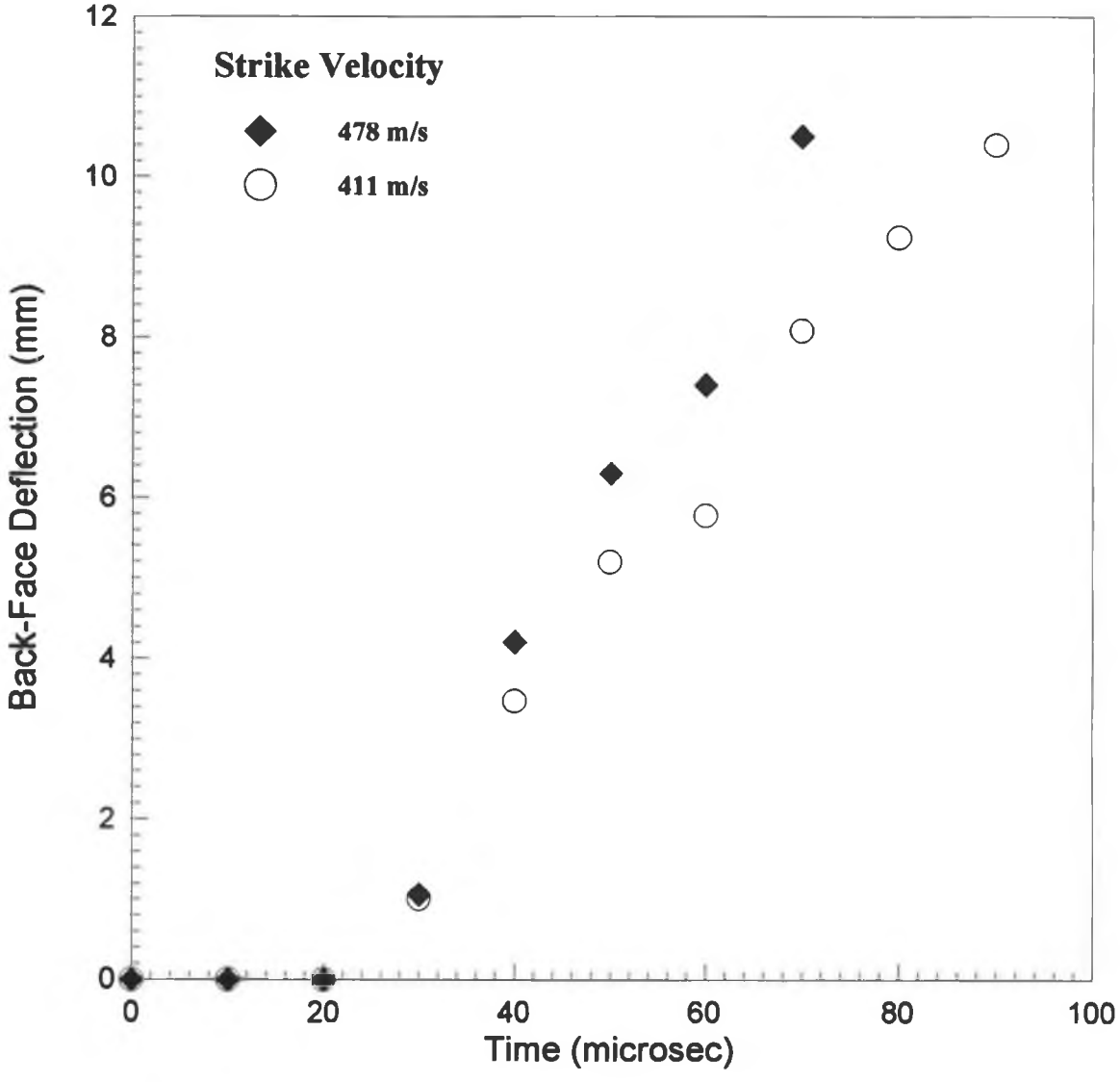

Figure 12. Back-face deflection of S-2 glass laminates impacted by a hemispherical nose projectile.

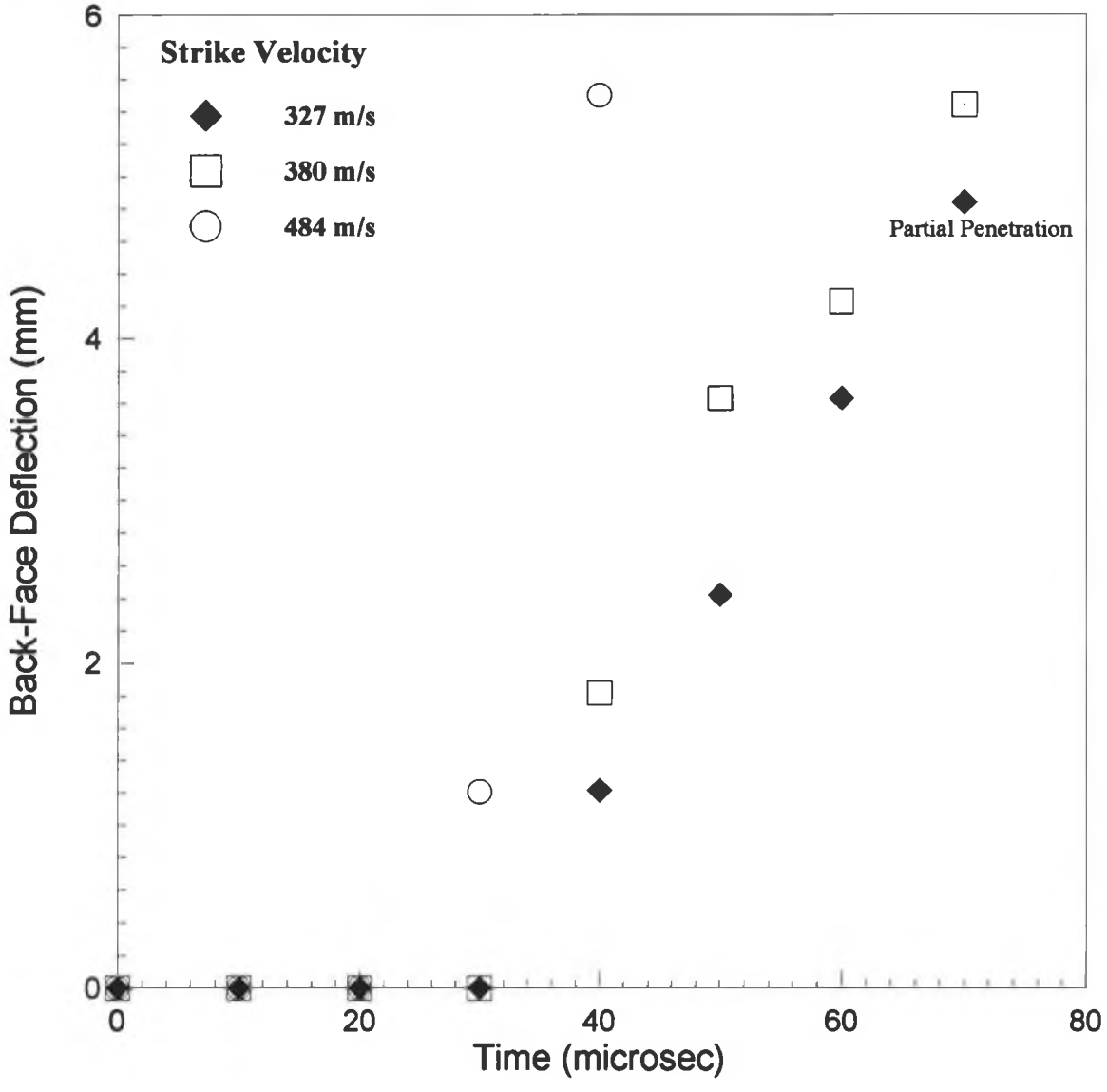

Figure 13. Back-face deflection of S-2 glass laminates impacted by a conical nose projectile.

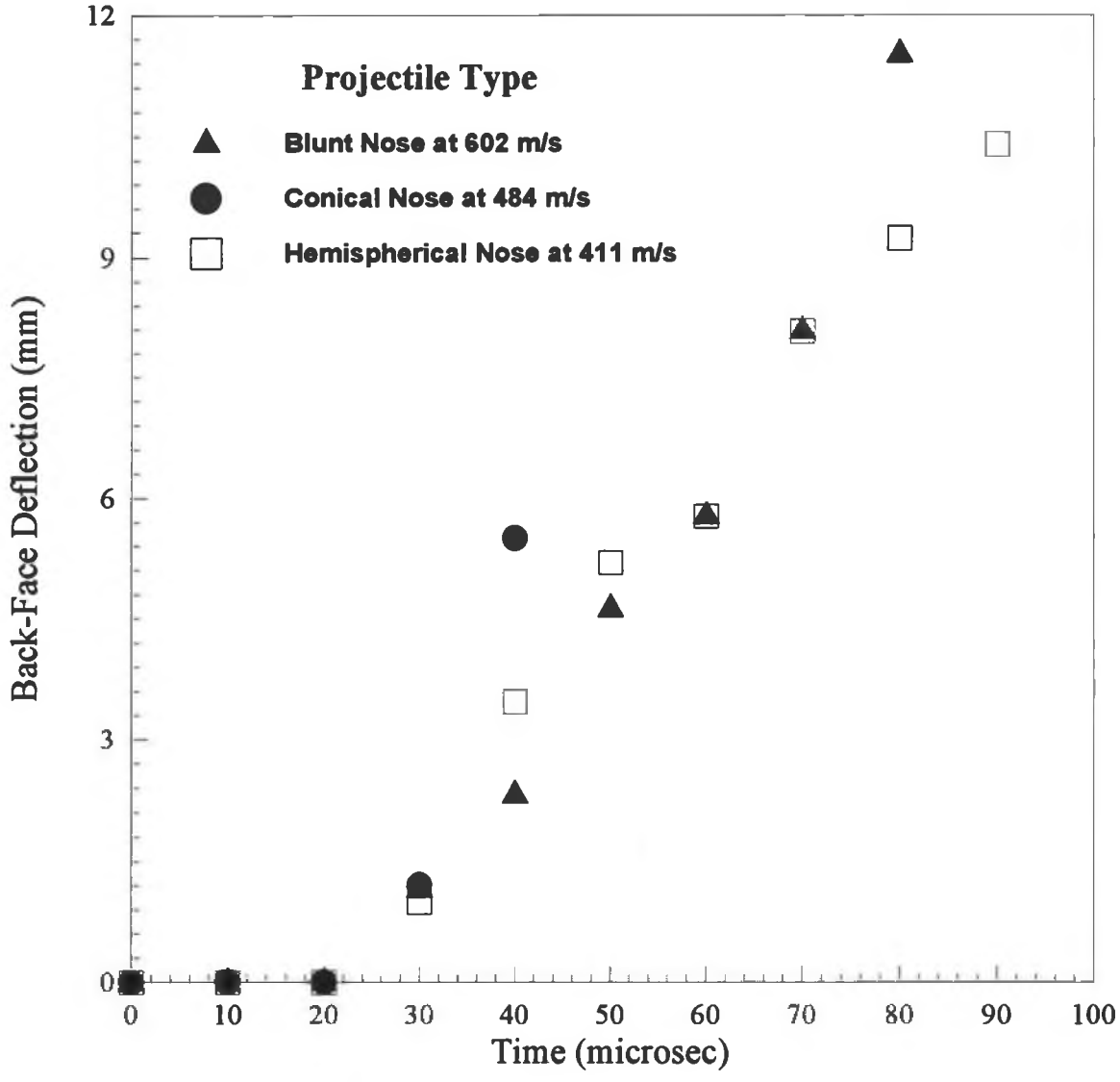

Figure 14. Comparison of back-face deflection of the laminates impacted by all three type of projectiles.

CHAPTER IV
FAILURE CRITERIA

4.1 GENERAL

The failure modes observed in composite laminates subjected to impact loading are very complex and the failure criteria based on the observed failure modes during penetration and perforation of the laminates are scarce. Lee and Sun assumed in their study, the initiation of matrix cracking occurred when the stress normal to fiber direction reaches its tensile strength and that leads to delamination of laminates [16].

Chang-Chang developed failure criteria based on the failure modes (fiber failure, matrix cracking and matrix crushing) in experiments from tensile loading of the bolted joints of the laminates (Appendix A) [23]. These failure criteria were incorporated in a finite difference code developed by them and successfully predicted the failure modes of the bolted joints. Whirley incorporated these failure criteria in DYNA3D [22]. Blanas simulated to predict the ballistic limit of the composite laminates against 5.8, 17 and 44 grain FSPs using these failure criteria in DYNA3D [21]. Simulations were also performed to predict the residual velocity of the projectiles. The simulations did not agree with the measured results and are discussed in chapter VI.

4.2 PROPOSED FAILURE CRITERIA

To the author's knowledge, no failure criteria are available for the failure modes observed in penetration of composite laminates for the velocity range (400 to 600m/s). The observed failure modes, cratering, fiber stretching and breaking, delamination and laminate crushing in 12.7 mm thick S-2 glass laminates impacted by 7.9 mm caliber FSPs

are discussed in Chapter III. A stress based failure criteria are proposed for the failure modes observed and are given below.

1. Cratering Failure

The laminates shear around the projectile and a crater is formed in the target. When, the transverse shear stress σ_{zx} is equal or exceeds the transverse shear strength S_{zx} of the laminate failure by cratering occurs. Thus the cratering failure is defined by

$$\sigma_{zx} \geq S_{zx} \tag{5}$$

2. Fiber Stretching and Breaking

The fibers stretch and break during penetration process. The normal stress σ_{xx} and the transverse shear stress σ_{zx} subject the fiber to tension. When these stresses exceed the normal tensile strength X_t and S_{zx} of the laminate, this type of failure occurs. The proposed failure criteria for fiber stretching and breaking is

$$\frac{\sigma_{xx}^2}{X_t^2} + \left(\frac{\sigma_{zx}}{S_{zx}}\right)^2 \geq 1.0 \tag{6}$$

3. Delamination

Delamination occurs when the stress in the transverse direction reaches the laminates tensile strength. This type of formulation has been used to study delamination in low velocity impact as well as in impact penetration of composites [16]. Thus delamination will occur when

$$\sigma_{zz} \geq Z_t \tag{7}$$

4. Laminate Crushing

During penetration the sheared laminates around the projectile are being compressed and crushed. This takes place due to combination of stress which exceeds the transverse shear stress and compressive stress in the thickness direction. Compressive failure in matrix was predicted using Hashin failure criterion [24], the modified form of the equation is

$$\frac{\sigma_{zz}^2}{4S_{zx}^2} + \left(\frac{Z_c^2}{4S_{zx}^2} - 1\right)\left(\frac{\sigma_{zz}}{Z_c}\right) + \frac{\sigma_{YZ}^{\ 2}}{S_{zx}^2} \geq 1.0 \qquad (8)$$

Where Z_C is the transverse compressive strength in the thickness direction of the laminate.

CHAPTER V
NUMARICAL SIMULATIONS

5.1. GENERAL

A number of analytical and computational models are available in studying isotropic materials under impact penetration and a comprehensive review of these studies can be found in [1-3]. However, the analytical modeling of composite laminates is very difficult due to anisotropic nature of the laminates and together with complex failure modes in the laminates during penetration of a projectile. Hence, FEM modeling of the impact phenomena on composite laminates through finite element simulations is a very important tool to predict the ballistic limit of the laminates and residual velocity of the projectiles. However, these studies are in the preliminary stage due to difficulties in deriving the proper failure criteria to predict the measured results on ballistic penetration into composite laminates.

The present simulation study consists of i) initial simulations are performed on the back-face deflection of HY100 plate impacted by 4340 steel projectile at two velocities 149 and 169 m/s to validate the DYNA3D code calculations [25], ii) to simulated ballistic limit and residual velocity of the blunt nose projectile penetrates 12.7 mm thick S-2 glass laminates using Chang and Chang failure criteria in DYNA3D, iii) to simulated ballistic limit and residual velocity of the blunt nose projectile penetrates 12.7 mm thick S-2 glass laminates using the proposed failure criteria given in Chapter IV, and iv) to simulate the ballistic limit of 6.4 mm thick S-2 glass laminates impacted by 5.8, 17 and 44 grain blunt nose projectiles (FSPs) in order to check the validity of the proposed failure criteria for laminates of other thickness.

5.2 DESCRIPTION OF DYNA3D CODE

The three dimensional finite element code called DYNA3D has been developed by Lawrence Livermore National Laboratory [22]. This code has a preprocessor called INGRID [26] to generate the FEM model and a post-processor TAURUS [27] used to analyze the results from DYNA3D. It has 41 material models, 11 equations of state and 12 general interface contacts. Three material models are available to study composite materials.

It is an explicit three-dimensional finite element code for analyzing the large deformation dynamic response of solids and structures. It is a Lagrangian code and follows the motion of fixed element mass. The computational grids are fixed in the materials and distort with them. Equations of motion are integrated in time explicitly using the central difference method. Spatial discretization is achieved by the use of following elements: 8 node solid hexahedron, 2 node beam, 4 node shell, 8 node solid shell, triangular shell and rigid bodies. DYNA3D has an extensive slide-line capability. Sliding interfaces are used where continuity of normal stress and velocity components between two surfaces is required. They are also used to provide movement of interface nodes between two surfaces that are expected to slide on each other.

Artificial viscosity is used to treat shock wave development and propagation. A pressure wave generally steepens until it propagates as discontinuous disturbance called shock. Shock leads to jumps in pressure, density, particle velocity and energy. The artificial viscosity method eliminates shock discontinuities by smearing the shock fronts over a small number of elements.

5.3 MODEL DESCRIPTION

5.3.1 Modeling on Steel Plate Impact

The geometry of the three dimensional model of 10mm thick HY100 steel target and (31mm diameter) x (89 mm long) 4340 steel projectile with flat nose is shown in Figure 15. The kinematic/isotropic elastic-plastic material model was used for modeling the flat nosed projectile and target. Due to axis of symmetry of the plate and the projectile one-fourth of the geometry was used to reduce the calculation time. The outer edge of the plates were fixed. A fine mesh geometry near the impact zone of the plate and projectile, and coarse mesh geometry for rest of the plate were used. The material properties are given in Table 2. The simulations were performed for two strike velocities 149 and 169 m/s. The nodal deflection histories, and energy histories of the system were acquired from the simulation using TAURUS [27]. The analysis was performed for 250 μs after impact.

5.3.2 Modeling on Composite Laminates

The dimensions of the woven S-2 glass/phenolic laminated plate are 15.24 x 15.24 x 1.27 cm. The diameter of blunt nose steel projectile was 0.76 cm with a nominal mass of 4.5 g. The tail of the projectile was not considered in modeling, but its was included in the projectile mass.

Figure 16 shows the geometry of the three dimensional model of the composite target and the blunt nose projectile. The model was generated using the preprocessor INGRID [26]. An 8 node solid hexahedron element was used to model both composite laminate and FSP. Due to axis of symmetry of the plate and the projectile one-fourth of the geometry was used to reduce the calculation time. The outer edge of the plates were fixed. A fine mesh geometry near the impact zone of the plate and projectile, and coarse mesh geometry for rest of the plate were used.

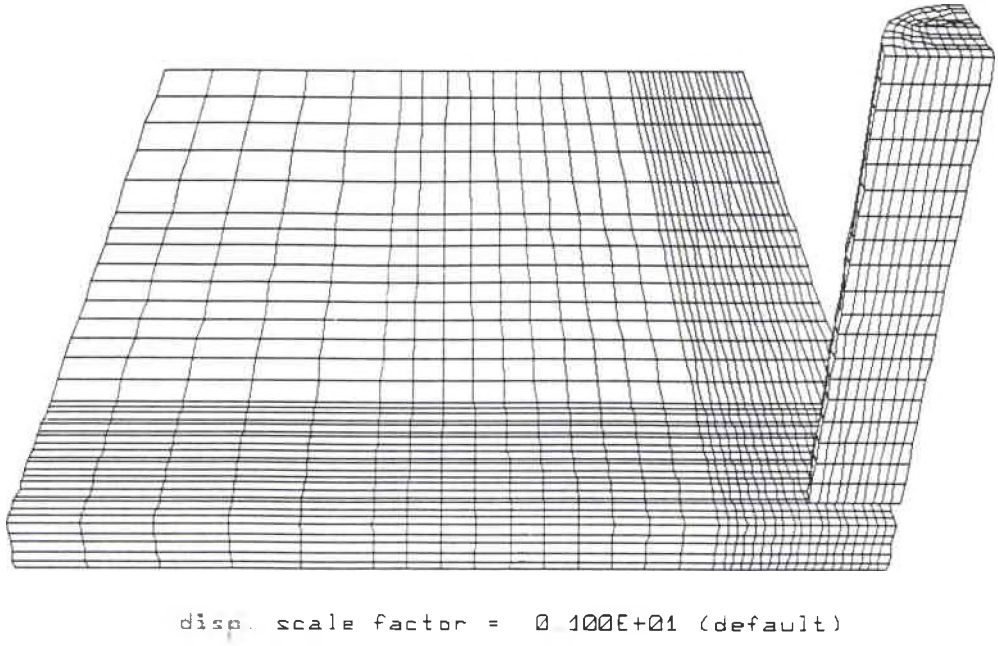

Figure 15. Three dimensional FEM model for HY100 steel plate and 4340 steel projectile

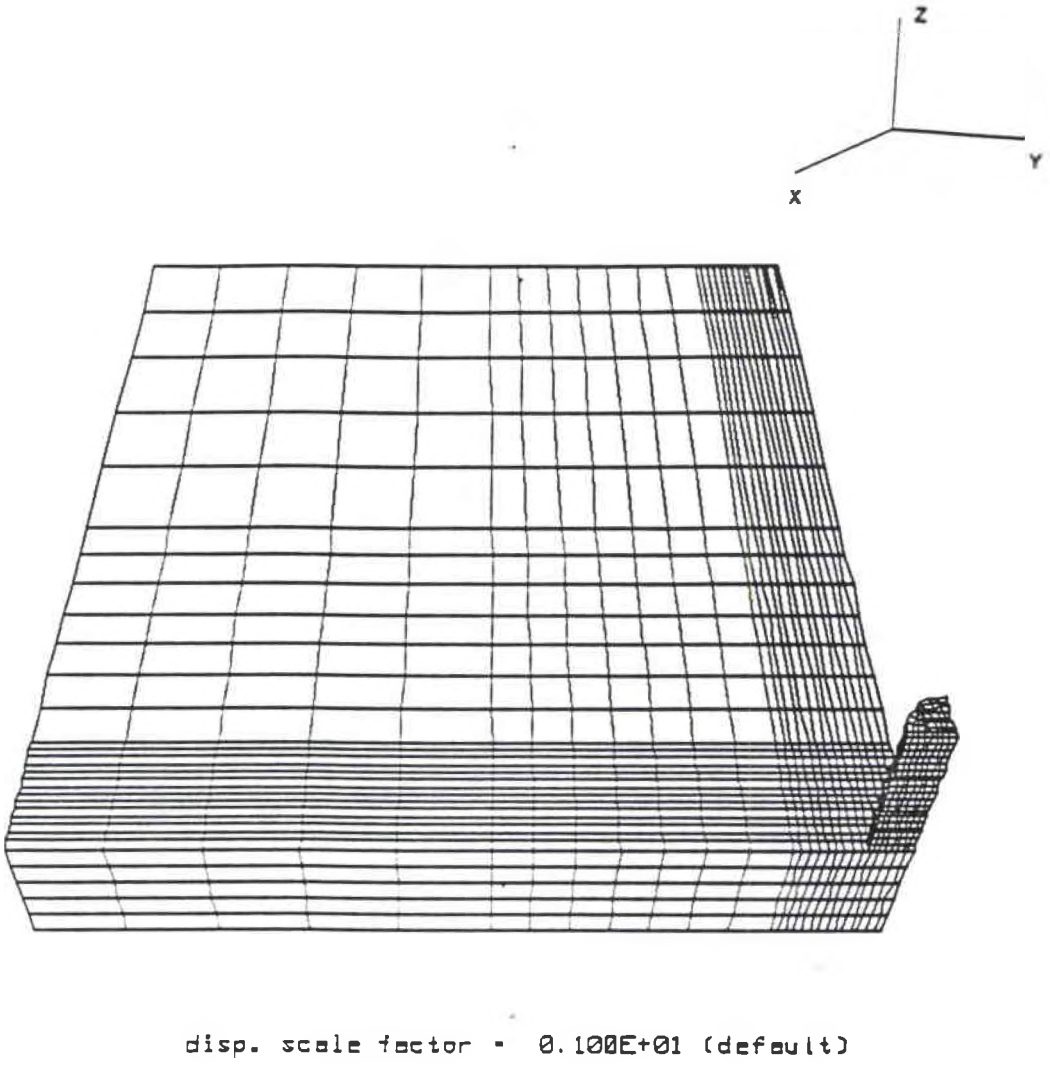

Figure 16. Three dimensional FEM model for composite plate and blunt nose projectile

Table 2

Mechanical properties of the HY100 steel plate and 4340 steel rod

	HY100 Steel	4340 Steel
Young's Modulus, E (GPa)	206.8	206.8
Poisson's Ratio, υ	0.3	0.3
Yield Stress, σ_0 (GPa)	0.79	1.103
Tangent Modulus, E_T (GPa)	-	0.827
Hardening Parameter, β	-	0.0

Table 3

Mechanical properties of the S-2 glass laminates and 4340 steel rod

Projectile: Material : SAE 4340 Steel

Young's Modulus, E (GPa)	206.8
Poisson's Ratio, υ	0.3
Yield Stress, σ_0 (GPa)	1.103
Tangent Modulus, E_T (GPa)	0.827
Hardening Parameter, β	0.0

Target: S-2 Glass composite [21, 28].

Longitudinal Modulus, E_x (GPa)	31.72
Lateral Modulus, E_y (GPa)	31.72
Transverse Modulus, E_z (GPa)	11.7
Shear Modulus, G_{xy}, G_{yz}, and G_{zx} (GPa)	7.5
Poisson's Ratio	
ν_{xy}	0.1
ν_{zy}, ν_{zx}	0.14
Tensile Strength, X_t and Y_t (MPa)	828
Shear Strength (inplane), S_c (MPa)	552
Transverse Shear strength, S_{zx} and S_{yz} (MPa)[29]	63.2
Tensile Strength from unidirectional laminate Z_t (MPa)	83
Compressive Strength Z_c (MPa)	750
Density, g/cc	1.8

A kinematic/isotropic elastic-plastic material model for the flat nosed projectile and the composite damage material model for the composite laminate were used. The material model constants for the composite target and steel projectile utilized in this study are given in Table 3 [21, 28]. It was assumed that inplane and transverse shear modulii are same for the laminates. The transverse shear strength of S-2 glass laminate was obtained from [29].

Simulations are performed using the VAX at the University of Dayton and the Ohio State CRAY-YMP computer and analysis was carried out for maximum of 100 μs. The data obtained at the end of each simulation using the post-processor TAURUS are : i) energy histories of the system, projectile and target, 2) displacement and velocity histories of nodes, 3) velocity history for the projectile, 4) element stress histories and 5) contour stress plots.

CHAPTER VI

RESULTS AND DISCUSSIONS

6.1 PENETRATION THROUGH STEEL PLATE

The back-face deflection of HY100 steel plates measured using the Imacon high speed camera at a framing rate of 10^5f/s are shown in Figure 17 for two strike velocities 149 and 169 m/s [25].

The displacement history of the central node located at the back side of the target below the impact site, is shown in Figure 17. The simulated value of deflection are in good agreement with the measured values. This agreement validates the DYNA3D code calculation for isotropic materials.

6.2 PENETRATION IN COMPOSITE LAMINATES

Initial analysis are performed to check the effect of the number of elements through the thickness of the laminates and to study the transverse shear stress distribution through the thickness of the laminates. Kinetic energy of the system after the impact and the maximum normal stress in the Z-direction are calculated to check the effect of the number of elements through the thickness of the laminates. Simulations are performed with 5, 11, 19, and 29 elements through the thickness of the laminates at the strike velocity 466 m/s. Transverse shear stresses through the thickness of the laminates at (0, 3.9 mm) where the projectile radius meets one edge of the plate, normal stress in Z-direction for the first element (at (0,0)) on the impact side of the laminates and the kinetic energy of the system after impact are recovered at the end of each simulation.

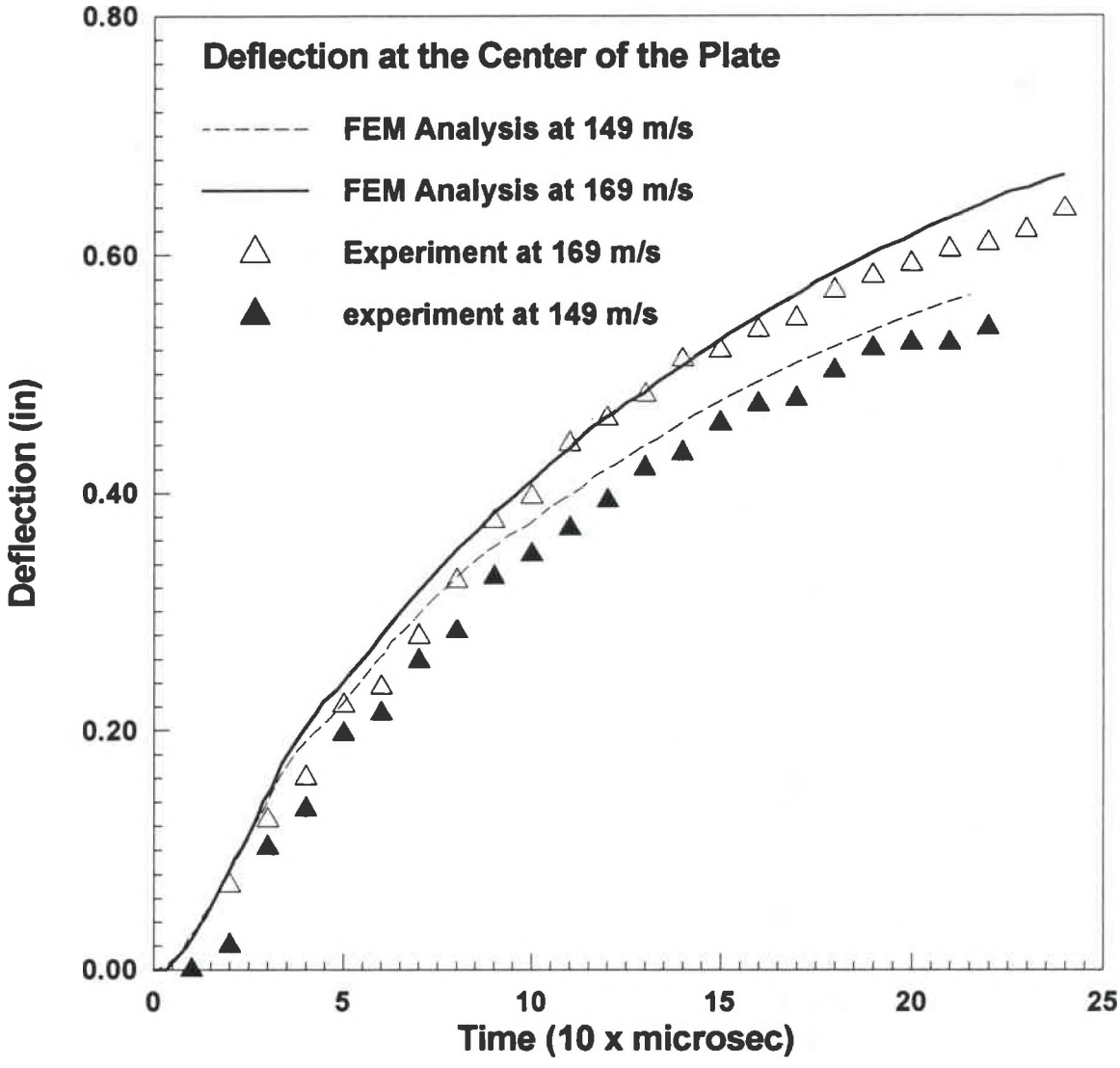

Figure 17. Comparison of simulated and measured back-face deflection of HY100 plate impacted by a projectile at two velocities

The transverse shear stresses at 5 μs after impact of the projectile and the normalized thickness of the laminate are plotted in Figure 18. The transverse shear stress distribution is skewed parabolic, and becomes relatively smooth as the number of elements through the thickness increased to 29 (Figure 18). The magnitude of maximum transverse shear stress remains constant. The skewed distribution of the transverse shear stress shown in Figure 18 agrees with the requirement that the transverse stress distribution through the thickness of the laminates should be parabolic.

The kinetic energy of the system after impact is 10.5 J is independent of number of elements, 5, 11, 19 and 29 through the thickness of the laminate. The magnitude of normal compressive stress σ_{zz} in the first element of the laminate is about 1.65 GPa and does not depend on the number of elements through the thickness of the laminates.

Immediately after the impact of the projectile, the response of the composite materials is highly localized. Material in front of the projectile is subjected to a compressive stress. During this time, composite laminates around the projectile is subjected to high transverse shear stresses. Penetration is initiated by laminate crushing, results due to transverse shear stress and normal compressive stress in the z-direction. Figures 19 and 20 show contour of transverse shear and normal stresses in the z-direction distribution in the target and projectile. This agrees with the observation summarized in Chapter III.

Table 4 lists the predicted residual velocities of the projectile with different combinations of Chang-Chang failure criteria for fiber failure, matrix failure, matrix crushing and delamination from simulations at different strike velocities. The predicted residual velocity of the projectiles and ballistic limit of the laminates based on the proposed failure criteria for cratering, fiber stretching and breaking, laminates crushing and delamination are listed in Table 5.

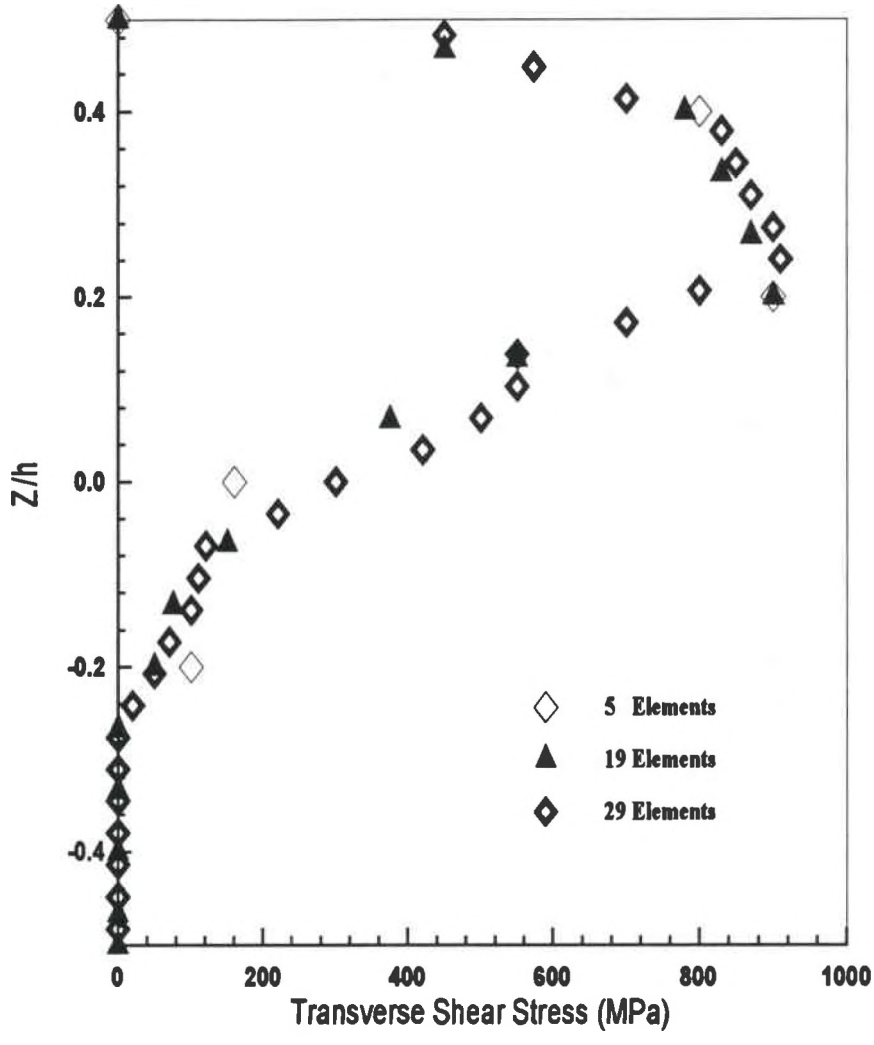

Figure 18. Transverse shear stress distribution through the thickness of the laminates

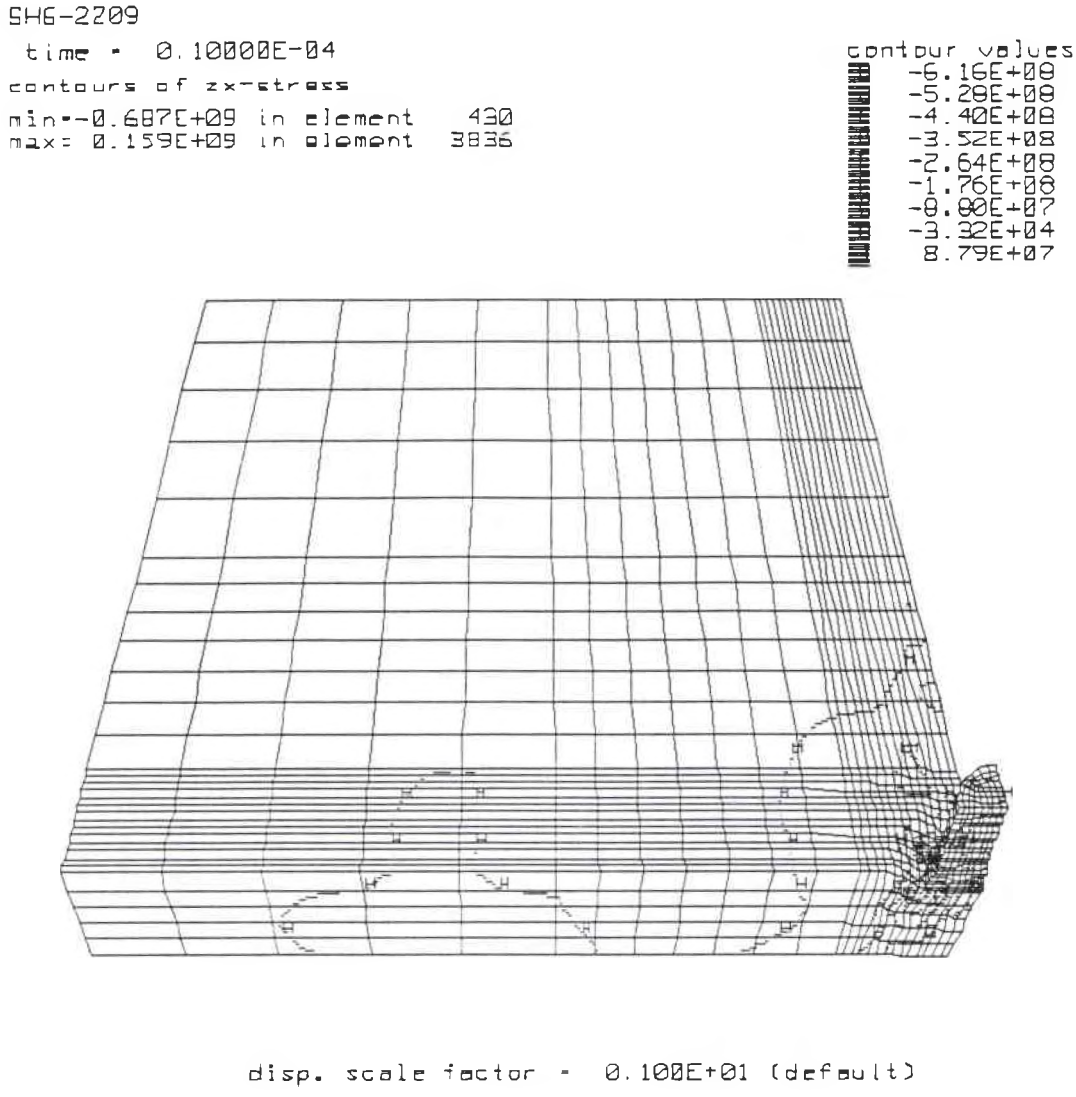

Figure 19. Transverse shear stress contour at 10 μs after impact.

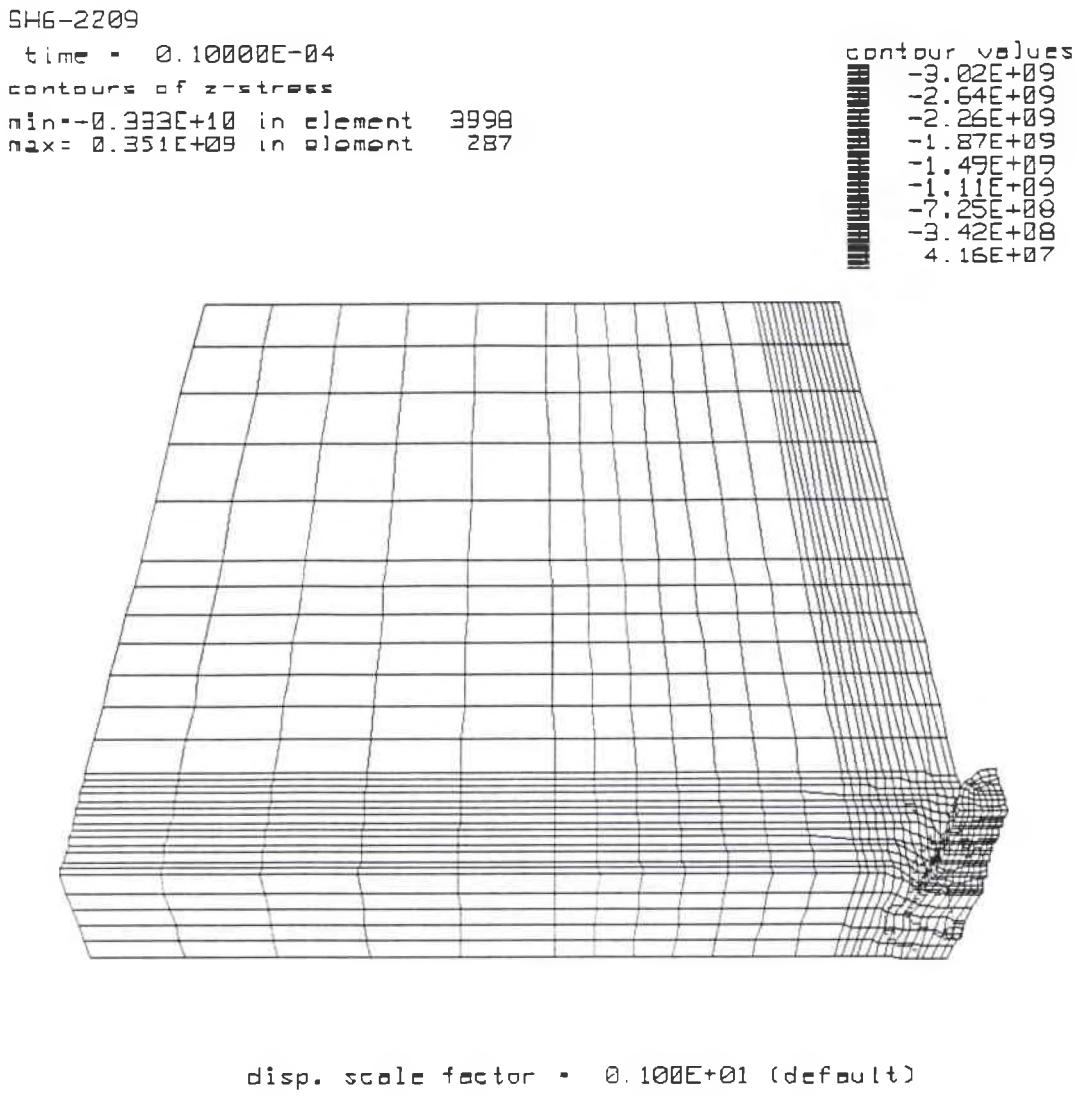

Figure 20. Normal stress (σ_{zz}) contour at 10 μs after impact.

Table 4
Residual velocities of the blunt nose projectile impacted on to 12.7 mm S-2 glass laminates from simulations using Chang-Chang failure criteria and experiments

Shot No.	Velocity(m/s)	V_r (m/s) from different failure criteria				
		1, 2 & 3	1, 2 & 4	1,& 2,	1, 2, 3, & 4	Experiment
SH2195	602	278	-	282	-	-
SH2196	612	240	405	245	405	-
SH2209	466	131	213	139	213	0
SH2213	571	195	349	202	349	310

1- Fiber breakage, 2-matrix cracking, 3- matrix crushing failures and 4-delamination failures [26]

Table 5
Residual velocities of the blunt nose projectile impacted on to 12.7 mm S-2 glass laminates from simulations using proposed failure criteria and experiments

Shot No.	Velocity(m/s)	V_r (m/s) from different failure criteria			
		1, 4	2 and 3	1, 2, 3, and 4	Experiment
SH2209	466		0	0	0
SH2210	520		0	125	0
BL#	533	50	0	250	0
SH2211	547	50	65	50	80
SH2213	571	300	-	300	310

Ballistic Limit of 0.5" S-2 glass laminates
1- Fiber stretching and breaking, 2-laminate crushing, 3-delamination, and 4- cratering failures

The predicted residual velocities of the projectile for different combinations of Chang-Chang failure criteria are given in Table 4. The simulations did not predict the ballistic limit correctly and the residual velocity at a strike velocity of 571 m/s was 37% lower than the measured values following the failure criteria for fiber failure, matrix failure and matrix crushing. Fiber failure and matrix failure predicted the residual velocities 34% lower than the measured values. This suggests that the laminate crushing has little or no effect on the predicted residual velocities of the projectile, since this failure criteria is defined using the stresses τ_{xy} and σ_{yy} which are fiber dominated properties for woven composite laminates.

The failure criteria for delamination available in DYNA3D has been defined using the stresses τ_{zx}, τ_{yz} and σ_{zz}. The stresses τ_{zx} and τ_{yz} do not play any role in predicting delamination during penetration process, since these stresses participate in cratering and fiber stretching and breaking failures. In impact studies delamination is described using the tensile normal stress σ_{zz} [16]. Using the failure criteria where all fiber modes matrix failure, matrix crushing and delamination are activated and the predicted residual velocities are higher than those of the previous predictions for strike velocities below and above the ballistic limit of the target (Table 4).

The proposed failure criteria for laminate crushing, fiber stretching and breaking, delamination and cratering are incorporated as part of composite damage material model in DYNA3D (Chapter IV) and simulations are performed to predict the ballistic limit of the target. Initially, cratering and laminate crushing are activated and the ballistic limit predicted is incorrect. Laminate crushing and delamination failure criteria predicted the ballistic limit as shown in column 4 of Table 5. Furthermore the combination of laminate crushing and delamination predicted the residual velocity of the projectile above the ballistic limit of the target also showed good agreement with the measured values.

Above the ballistic limit the combination of cratering and fiber stretching and breaking are dominant (Chapter III). The predicted residual velocity of the projectile

based on these failure criteria are within 10% of the measured values (Table 5). Combination of all the four failure modes, fiber stretching and breaking, cratering, delamination, and laminate crushing as failure criteria predicted ballistic limit of the laminate is 15% lower. Above the ballistic limit of the laminates the residual velocities from the simulations agreed within 10% of the measured values. The nodal deflection of the laminates is also recovered from the simulations. The simulated back-face deflection of the laminate did not correlate at all with the measurements.

Simulations were also carried out to predict the ballistic limit of 6.4 mm thick S-2 laminates impacted by 5.8, 17, and 44 grain FSPs using the same failure criteria, laminate crushing and delamination. The predictions do not agree with the measurements, are given in Table 6.

Table 6
Residual velocities of the projectiles impacted on to 6.4 mm S-2 glass laminates from simulations using proposed failure criteria and experiment

FSP (Grains)	Velocity(m/s)	V_r (m/s) failure from different criteria	
		2 and 4	2 and 3
5.8	550		0
	621*	0	0
17.0	470*	0	60
	520	70	60
44	350*		60
	320		60
	380		60

* Ballistic Limit from experiment [21]

CHAPTER VII

CONCLUSIONS AND RECOMMANDATIONS

7.1 CONCLUSIONS

Failure modes in 0.5 inch thick S-2 glass composite impacted by 0.3 caliber FSPs with three different nose shape, blunt, conical and spherical nose shapes were identified as part of post failure analysis. Two different sets of failure modes are observed in the laminates for velocities above and below the ballistic limit. Cratering, delamination and laminate crushing were major failure modes in the target for velocities below the ballistic limit. On the contrary, for velocities above the ballistic limit of the laminates the failure modes were cratering, delamination, and fiber stretching and breaking. The extent of cratering decreased with increase in strike velocity. The measured back-face deflections of the laminates increased with strike velocity up to the ballistic limit of the target and remained almost constant above the ballistic limit of the laminates. The laminates impacted by blunt and hemispherical nose projectiles deflected 40% higher than conical nose projectile.

The predicted results from simulations using Chang-Chang failure criteria for fiber failure, matrix failure, delamination, and matrix crushing did not show good agreement with the experimental results. The proposed failure criteria based on observations of the shot targets showed good agreement with the measured ballistic limit of the laminates and the residual velocities of projectiles from the experiments. The proposed failure criteria failed to predict the ballistic limit of 6.4 mm thick S-2 glass laminates impacted by 5.8, 17, and 44 grain FSPs

7.2. RECOMMENDATIONS

7.2.1 Experiments

Penetration/perforation of laminated panels is a very complicated phenomena compared to the penetration/perforation in isotropic materials. The penetration/perforation process in laminates involves failure modes such as fiber stretching and failure, delamination, and matrix failure. The failure modes depend on the type of composite laminates, type of projectile and strike velocity.

Furthermore the impacted laminates undergo bulging around the penetration cavity. The bulging is likely to be a function of the lateral dimension of the panel. Fraction of the kinetic energy of the projectile is absorbed by the bulging process. Carefully planned experiments are recommended to account for the bulging during penetration. Experiments under well defined strain or stress conditions should be performed. One dimensional strain or plate impact experiments with embedded stress gauges are likely to provide valuable data on matrix cracking, fiber failure and delamination of composite laminates. One dimensional stress experiments using split Hopkinson bar will also provide data on matrix crushing in compression mode, fiber stretching and breaking in tensile mode.

7.2.2 Analysis

Computer simulation of the stress-time profiles obtained in plate impact (1-d strain) and Hopkinson bar data on tensile and compressive behavior of composites should be performed. These simulations will provide some insight into the validity of the material models and failure criteria used in simulations. In the event if these simulations are successful, simulation of penetration problem should be attempted using proper material models.

APPENDIX - A

AVAILABLE FAILURE CRITERIA IN DYNA3D

Chang and Chang proposed failure criteria based on the failure modes observed in experiments on bolted joints of the laminates [23]. Plane stress conditions were assumed and three different inplane failure modes were considered: fiber breakage, matrix cracking, and matrix crushing. In addition to these a failure model to account for delamination is also included in DYNA3D. This is not activated during the analysis in the original code. DYNA3D uses the same failure criteria for each element since the one point integration is used for 8 node hexahedron solid element. The failure models are described below:

Fiber Breakage

The fiber breakage is defined as

$$e_f = \frac{\max(0,\sigma_{xx}^2)}{X_t^2} + \frac{\frac{\sigma_{xy}^2}{2G_{xy}} + \frac{3}{4}\alpha\sigma_{xy}^4}{\frac{S_c^2}{2G_{xy}} + \frac{3}{4}\alpha S_c^4} \leq 1.0 \qquad \text{(A-1)}$$

Where σ_{xx} (Positive) and σ_{xy} are longitudinal and shear stresses in the ply, G_{xy} is the initial ply shear modulus, X_t is the longitudinal tensile strength, α is the constant that is to be determined experimentally and S_c is the in-situ ply shear strength measured from a cross-ply laminate, $[0/90]_s$, with the same thickness as the laminate considered.

For laminates with linear elastic behavior, $\alpha = 0$ and the equation reduces to

$$e_f = \frac{\max(0,\sigma_{xx}^2)}{X_t^2} + \frac{\sigma_{xy}^2}{S_c^2} \leq 1.0 \qquad \text{(A-2)}$$

The fiber breaking occurs if $e_f > 1.0$

Matrix Cracking

Matrix cracking is defined as

$$e_m = \frac{\max(0,\sigma_{yy}^2)}{Y_t^2} + \frac{\frac{\sigma_{xy}^2}{2G_{xy}} + \frac{3}{4}\alpha\sigma_{xy}^4}{\frac{S_c^2}{2G_{xy}} + \frac{3}{4}\alpha S_c^4} \leq 1.0 \qquad \text{(A-3)}$$

Where σ_{yy} (positive) is the stress in the lateral direction, and Y_t is the lateral tensile strength.

For laminates with linear elastic behavior, $\alpha = 0$ and the equation reduces to

$$e_m = \frac{\max(0,\sigma_{yy}^2)}{Y_t^2} + \frac{\sigma_{xy}^2}{S_c^2} \leq 1.0 \qquad \text{(A-4)}$$

The matrix cracking occurs if $e_m > 1.0$

In this study, the above failure modes are same since the considered laminate was woven fabric for which modulii $E_x = E_y$ and the tensile strength $X_t = Y_t$.

Matrix Crushing

Matrix failure in compression is predicted by Hashin Failure criterion

$$e_d = \frac{max(0,\sigma_{yy}^2)}{4S_c^2} + \left(\frac{Y_c^2}{4S_c^2} - 1\right)\left(\frac{\sigma_{yy}}{Y_c}\right) + \frac{\frac{\sigma_{xy}^2}{2G_{xy}} + \frac{3}{4}\alpha\sigma_{xy}^4}{\frac{S_c^2}{2G_{xy}} + \frac{3}{4}\alpha S_c^4} \leq 1.0 \qquad \text{(A-5)}$$

Where Y_c is the lateral compressive strength of the unidirectional ply.

For linear elastic laminates equation becomes

$$e_d = \frac{max(0,\sigma_{yy}^2)}{4S_c^2} + \left(\frac{Y_c^2}{4S_c^2} - 1\right)\left(\frac{\sigma_{yy}}{Y_c}\right) + \frac{\sigma_{xy}^2}{S_c^2} \leq 1.0 \qquad \text{(A-6)}$$

Matrix crushing occurs if $e_d > 1.0$

Delamination

Delamination is defined by the equation

$$e_l = \frac{max(0,\sigma_{zz}^2)}{Z_t^2} + \left(\frac{\sigma_{yz}}{S_{yz}}\right)^2 + \left(\frac{\sigma_{zx}}{S_{zx}}\right)^2 \leq 1.0 \qquad \text{(A-7)}$$

Where σ_{zz} (Positive), σ_{zx} and σ_{yz} are transverse shear stresses, Z_t is the normal tensile strength in the thickness direction, and S_{zx} and S_{yz} are transverse shear strengths. In this study the transverse shear strength of S-2 glass/epoxy is used [29]. The error in the source code of DYNA3D was corrected in order to account for this failure.

Delamination occurs if $e_l > 1.0$

REFERENCES

1. Backman and Goldsmith, The Mechanics of Penetration of the Projectiles, Int. J. Engng. Sci., Vol. 16, 1-99 (1978).

2. High velocity Impact Dynamics, ed. Zukas, John-Wiley and sons, 1990.

3. Impact Dynamics, Zukas et al., John-Wiley and sons, 1984.

4. Anderson, C. E., and Bordner, S. R., Ballistic Impacts: the Status of Analytical and Numerical Modeling, Int. J. Impact Engng., Vol. 7, No. 1, 9-35 (1988).

5. Anderson, C. E., An Overview of the Theory of Hydrocodes, Int. J. Impact Engng., Vol. 5, 33-59 (1987).

6. Prevorsek, D. C., Chin, H. B., and Bhatnagar, A., Damage Tolerance: Design for Structural Integrity and Penetration, Composite Structures, Vol. 23, 137-148 (1993).

7. Cantwell, W. J., The Influence of Target Geometry on the High Velocity Impact Response of GFRP, Composite Structures, Vol. 10, 247-265 (1988).

8. Cristescu, N., Malvern, L. E., and Sierakowski, Failure Mechanisms in Composite Plates Impacted by Blunt-Ended Penetrators, Foreign Object Impact Damage to Composites, ed. Greszczuk, L. B., ASTM STP 568, pp 159-172, American Society for Testing and Materials, Philadelphia, 1975.

9. Merriman, E. A., and Miner, L. H., Fragmentation Resistance of Fiber Reinforced Ballistic Structures, Proceedings from the Tenth International Symposium on Ballistics, Vol. - II, San Diego, Oct. 27-29, 1987.

10. Benyami, M., Bless, S. J., and Jurick, D. L, Techniques to Study Penetration through Glass Reinforced Phenolic, Presented at the Aeroballistic Range Association in San Diego, CA, Oct. 1990.

11. Bless, S. J., Benyami, M., and Hartman, D., Penetration through Glass-Reinforced Phenolic,22nd SAMPE Technical Conference, Boston, November 1990.

12. Bless, S. J., Hartman, D., and Hanchak, S. J., Ballistic Perforation of Thick S-2 Glass Composite, UDR-TR-85-88A, University of Dayton Research Institute, Dayton, OH 45469.

13. Bless, S. J., KRP Test Report, UDR-TM-86-06, University of Dayton Research Institute, Dayton, OH 45469.

14. Bless, S. J., Rondeau, R., and Strader, E., Fabrication and Testing of Composite Targets, UDR-TR-86-138, University of Dayton Research Institute, Dayton, OH 45469.

15. Dynamic Response of S-2 Glass Reinforced Plastic Structural Armor, Eds. Chou, S. C., and DeLuca, E., Report No. ARL-SR-5, Army Research Laboratory, Dec. 1993.

16. Lee, S. W. R., and Sun, C. T., Ballistic Limit Prediction of Composite Laminates by Quasi-Static Penetration Model, 24th SAMPE Technical Conference, Oct. 20-22 1992.

17. Hsieh, A., Jang, B. Z., and Zee, R. F., Response of Polymer Composites to High and Low Velocity Impact, 22nd International SAMPE Technical Conference, Nov. 6-8, 1990.

18. Zhu, G., Penetration of Laminated Composites by Projectiles, Ph. D. Dissertation, University of California, Berkeley, 1990.

19. Cantwell, W. J., and Morton, J., Impact Perforation of Carbon Fiber Reinforced Plastic, Composite Science and Technology, Vol. 38, 119-141 (1990)

20. Lin, L. C., and Bhatnagar, A., Ballistic Energy Absorption of Composites - III, 24th International SAMPE Technical Conference, Oct. 20-22, 1992.

21. Blanas, A. M., Finite Element Modeling of Fragment Penetration of Thin Structural Composite Laminates, Report No. NATRICK/TR-22/019, U. S. Army Natrick Research, Natrick, MA. Dec. 1990.

22. Whirley, R. and Engelmann, B. E., DYNA3D: A Nonlinear, Explicit, Three-Dimensional Finite Element Code for Solid and Structural Mechanics - Users Manual, UCRL-MA-107254, Lawrence Livermore Laboratory, November 1993.

23. Chang, F. K., and Chang, K. Y., Post-Failure Analysis of Bolted Composite Joints in Tension or Shear-out Mode Failure, J. of Composite Material, Vol. 21, 809-833 (1987).

24. Hashin, Z., Failure Criteria for Unidirectional Fiber Composites, J. Appl. Mech., Vol. 47, 329-334 (1980).

25. Brar, N. S. and Hanchak, S. J., Unpublished Results, University of Dayton Research Institute, Dayton, OH 45469, 1992.

26. Christon, A. M., INGRID, 3-D Mesh Generator for Modeling Nonlinear Systems, UCRL-MA-109790 (Draft), Lawrence Livermore Laboratory, September 1992.

27 Thomas, S., TAURUS: An Interactive Post-Processor for the Analysis Codes, NIKE3D, DTNA3D, AND TOPAZ3D, UCRL-MA-105401, Lawrence Livermore Laboratory, May 1991.

28. Hartman, D. R., Typical Properties for S-2 Slass Fiber Laminates, Personal Communication, Owens Corning Fiberglass, Granville, Ohio, Jan. 1994.

29. Harding, J., Impact Damage of Composite Materials, Science and Engineering of Composite Materials, Vol. 1, No. 2, 41-68 (1989).